

Liege, July the 15<sup>th</sup>, 2016

# Tensile membrane action

Expert judgement about

the Bailey-Moore simple method and the software MACS+

2<sup>nd</sup> draft

*Jean-Marc Franssen*

Foreword : this document is a genuine report of the work that we performed, based on our most recent knowledge and with the best of our ability, free of any pressure from any kind. No result obtained has been concealed.

**Secteur Ingénierie Structurale (SE) / Ingénierie du feu**

Quartier Polytech 1, Allée de la Découverte 9 (Bât. B52/3) 4000 Liège (Belgique)

Tél. ++ 32 (04) 366 92 65

Email: [jm.franssen@ulg.ac.be](mailto:jm.franssen@ulg.ac.be)



This report is the second version presenting the results of our analysis of the Bailey-Moor simple method. Compared to the first version dated October 28, 2018:

- Some editorial and typing errors have been corrected.
- New geometries have been studied (6 x 6, 6 x 12, 9 x 12 and 9 x 15 m<sup>2</sup>).
- All simulations of SAFIR have been run with all variables of the concrete model in Double Precision
- The displacement criteria is evaluated from the initial configuration.
- Any reference to the version 2.0.6 of the software MACS+ has been delete as it is now obsolete. Only version 3.0.1 and 3.0.2 are discussed here.
- A mesh sensitivity has been added (2.2.2)

## Table of content

<b>1</b>	<b><i>The Bailey-Moore method</i></b> .....	<b>4</b>
1.1	<b>General overview</b> .....	<b>4</b>
1.2	<b>Detailed developments</b> .....	<b>8</b>
1.2.1	Estimation of the membrane forces .....	8
1.2.2	The enhancement factor .....	10
1.2.3	Estimation of the displacement .....	15
1.2.4	Contribution of the unprotected beams .....	15
1.3	<b>The FRACOF method</b> .....	<b>16</b>
<b>2</b>	<b><i>Numerical simulations</i></b> .....	<b>20</b>
2.1	<b>Thermal simulations</b> .....	<b>20</b>
2.1.1	Model of the composite slab.....	20
2.1.2	Model of the steel beams .....	23
2.1.3	Some results.....	25
2.2	<b>Mechanical simulations</b> .....	<b>26</b>
2.2.1	The model .....	26
2.2.2	Mesh sensitivity.....	28
2.2.3	7,5 x 15 m <sup>2</sup> .....	30
2.2.4	9 m x 9 m .....	36
2.2.5	6 m x 6 m .....	39
2.2.6	6 m x 12 m .....	40
2.2.7	9 m x 12 m .....	41
2.2.8	9 m x 15 m .....	43
2.2.9	3 sides heating versus 4 sides heating .....	44
2.2.10	Influence of lack of overlap.....	46
2.2.11	Effect of a localized fire.....	49
<b>3</b>	<b><i>Conclusions</i></b> .....	<b>53</b>
3.1	<b>Tensile membrane action</b> .....	<b>53</b>
3.2	<b>The Bailey-Moore simple method</b> .....	<b>53</b>
3.3	<b>The MACS<sup>+</sup> software</b> .....	<b>54</b>

3.4	Numerical modelling.....	55
4	<i>Bibliography</i> .....	56
5	<i>Annex: problems in the Bailey Moore simple calculation method</i> .....	57

# 1 The Bailey-Moore method

## 1.1 General overview

In this section, we present the main features and assumptions of the Bailey-Moore simple calculation method. This method is used to calculate the fire resistance with respect to the load bearing capacity performance R for floor slabs loaded by uniformly distributed vertical loads.

On the base of this method is the experimental observation that failure in the fire situation does not occur until very large displacements develop. At this ultimate stage, the failure mechanism is not anymore the “classical” yield lines mode where portions of the slab, assumed to be rigid, turn with respect to each other along linear yield lines in which only bending moments are present (no axial force) , see Figure 1<sup>1</sup>.



Figure 1: failure mode according to the yield line theory

At the ultimate stage in the fire situation, the deflection shows a double curvature shape, with both curvatures in the same direction and the radius of curvature varying continuously in the plane of the slab, see Figure 2.

---

<sup>1</sup> The four plates defined by the yield lines will be called here “the two trapezoidal plates” and “the two triangular plates”.

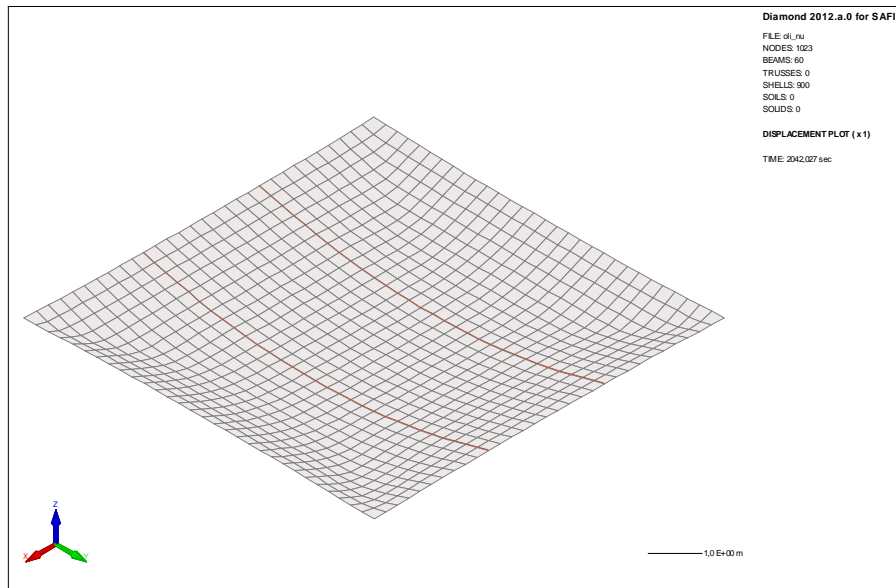


Figure 2: deflection calculated numerically

The central part of the slab behaves like a piece of fabric, a membrane, and is subjected essentially to “radial” tensile forces, while the external ring of the slab, near the vertical supports (that must be present on all 4 sides), is subjected to circumferential compression, see Figure 3. This behavior is only possible because;

- 1) tension in the central part of the slab is supported by a multidirectional continuous steel mesh;
- 2) compression in the external ring is supported by the reinforced concrete slab and;
- 3) the central part is anchored in the external ring.

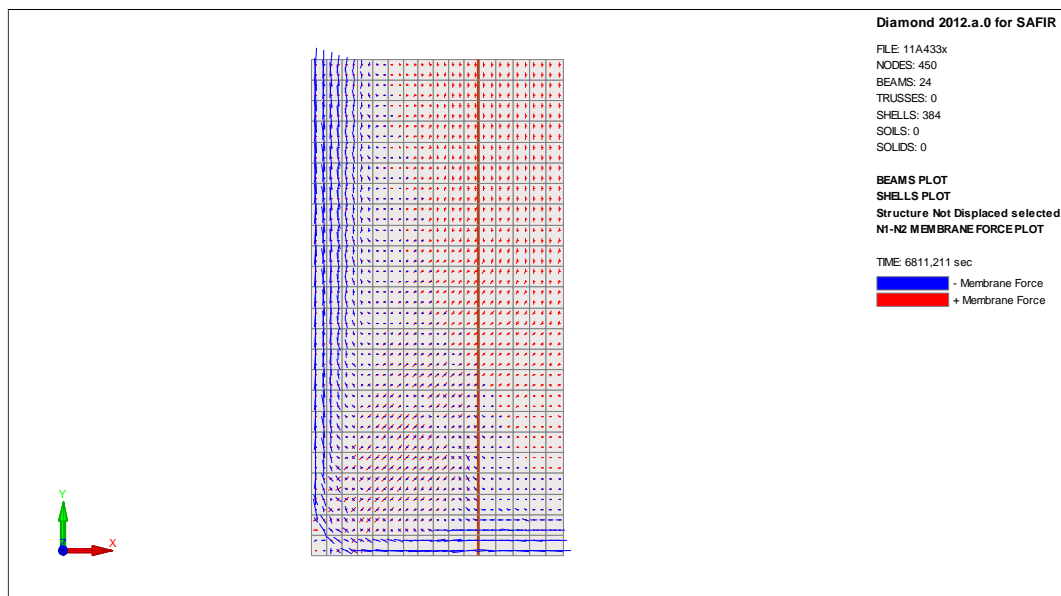


Figure 3: membrane forces in 1/4 of a slab panel after 104 minutes of fire

Nevertheless, the authors of the simple method take the deformed shape of the yield line theory and the ultimate load capacity calculated according to this theory as a starting point of their method. From there, they improve, they “enhance” in their terminology, the calculation of the ultimate

load bearing capacity taking into account the fact that tension/compression forces exist in these yield lines.

The development of the simple calculation method is schematically described hereafter.

1. Establish a method that takes into account the effect of membrane forces at room temperature, at least if the displacement at failure is known.
  - 1.1. Make a hypothesis about the kinematic of the slab when it deforms until failure: the slab deforms as it would if there is no membrane force, i.e. in the same manner as the one predicted by the bending yield line theory, see Figure 1.
  - 1.2. Make a hypothesis about the shape of the membrane force diagrams along the yield lines: membrane forces vary linearly along the yield lines, see **Erreur ! Source du renvoi introuvable.** in which membrane forces are drawn only for the upper trapezoidal plate.

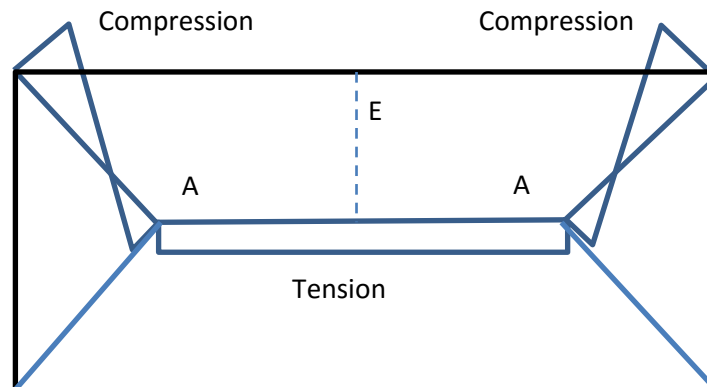


Figure 4: linear variation of membrane forces along yield lines

- 1.3. Make the hypothesis that the force is the same in the three yield lines at the point where they meet<sup>2</sup>, see point A on Figure 4.
- 1.4. From the equilibrium of the in-plane forces acting along the yield lines of the trapezoidal plate (as seen on Figure 4), calculate the relative amplitude of the membrane forces in the corners of the slab and at the intersection of the yield lines. At this stage, neither the failure load nor the amplitude of the membrane forces or of the displacements at failure is known.
- 1.5. Increase the membrane forces proportionally in the slab until they exceed some failure criteria, either tension in some re-bars or compression in the corners of the slab. Now, the amplitude of the membrane forces at failure is known, but not the failure load and not the displacement at failure.
- 1.6. Another equilibrium equation (moment of the membrane forces on the edges of half the trapezoidal plate about point E, see Figure 6) allows calculating the failure load of the slab, taking into account two favorable effects:

<sup>2</sup> This fact was already present in the very early papers of Hayes and it is not discussed anymore in the subsequent literature. As we have not been able to find a justification for that based on principles of structural mechanics, we assume that it is a hypothesis.

1.6.1. The fact that compressive membrane forces increase the resistance of the slab in bending around the yield lines<sup>3</sup> and;

1.6.2. The fact that membrane forces have a lever arm with respect to the supports, which reduces the demand in term of bending resistance along the yield lines.

Both effects depend on the amplitude of the membrane forces. The first one does not depend on the displacement  $w$  of the slab but the second one is proportional to this displacement. At this stage, the failure load  $P$  and the displacement  $w$  are not known but we have a linear relationship between both:

$$P = a + b w \quad (1)$$

where  $a$  and  $b$  are known positive constants. The failure load is thus bigger if larger displacements develop at failure.

In the terminology of the Bailey-Moore method, the failure load of the slab is expressed as an “enhanced” capacity compared with the failure load calculated on the base of the yield line theory  $P_0$ , i.e. when the membrane forces are not taken into account.

$$P = e P_0 \quad (2)$$

where  $e$  is the enhancement factor.

1.7. In fact, the enhancement factor is not calculated for the slab as a whole. Two enhancement factors  $e_1$  and  $e_2$  are calculated for the trapezoidal plates and for the triangular plates respectively. The two factors are then combined into one by the following equation:

$$e = e_1 + (e_2 - e_1) / (1 + 2 \mu r^2) \quad (3)$$

where  $r$  is the aspect ratio of the slab ( $L/l$ ) and  $\mu$  is the ratio of the moment capacity of the slab in orthogonal directions.

2. Extend this method to the fire situation.

2.1. Reduce the material properties of the steel re-bars depending on their temperature. The material properties influence the constants  $a$  and  $b$  that are present in equation 1.

2.2. Estimate the displacement at failure  $w$ , which will allow calculating the failure load from equation 1. This displacement is made of two components:

2.2.1. One from the thermal bowing due to the thermal gradient that appears on the thickness of the slab. The thermal curvature is estimated based on the short span of the slab.

2.2.2. One from the strain in the re-bars, assumed to be stressed at half the room temperature yield strength. This displacement is based on a parabolic deformed shape in the direction of the long span (but it is limited to 1/30 of the short span).

2.3. Tune<sup>4</sup> a little bit the estimation of the displacement to better correspond to the values that have been observed in full scale experimental tests made in Cardington.

3. Add to the load bearing capacity of the slab a term taking into account the effect of the internal unprotected steel beams. The bending resistance of these beams is considered.

---

<sup>3</sup> And, simultaneously, tensile forces in other parts of the slab reduce the bending strength.

<sup>4</sup> The displacement has been tuned *during the development of the method*. Designers don't have to tune their result for each application *when they apply the method*.

More details about the development of the method and the hypotheses that are being used are given in the following section.

## 1.2 Detailed developments

### 1.2.1 Estimation of the membrane forces

As rigid body turn with respect to each other along linear hinges, the hypothesis of rectangular compression stress block leads to the fact that the axial force perpendicular to a yield line varies linearly with the position of the neutral axis, see Figure 5, and, hence, varies linearly along the yield line, see Figure 4.

*Note: this is correct, as long as;*

1. *The neutral axis does not extend below the steel bar. If this occurs, there is a sudden variation of the compressive force. This situation could be present at the ends of the yield lines that end at the corner of the slab (that we will call "the corner lines"), where compression is the highest.*
2. *The neutral axis does not move up out of the section. If this occurs, there is no compressive stress and the tensile force becomes constant. This situation could be present in the central yield line (shown horizontally on Figure 4) and in some parts of the corner lines (near the central lines, point A on Figure 4).*

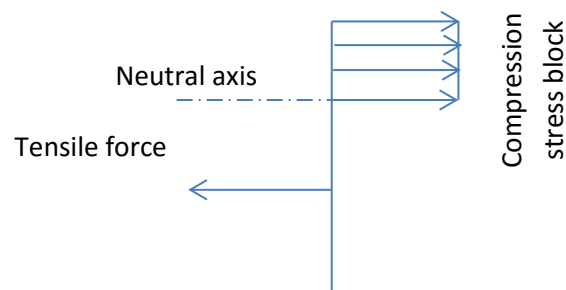


Figure 5: rectangular compression block

A relationship is then derived between the compressive resultant in the corner lines, the tensile resultant in the corner lines and the tensile resultant in the central line. This relationship comes from two equations of equilibrium of the rigid part shown on Figure 4.

In these equations, the resistance in tension of the steel reinforcing mesh per unit width is  $T_0$  in the direction parallel to the long edges of the slab and  $K T_0$  in the direction parallel to the short edges. The resistance in bending per unit width is  $M$  in the direction parallel to the long edges of the slab and  $\mu M$  in the direction parallel to the short edges.

*Note: in these two equations, the authors of the simple method consider that the resultant forces are horizontal. This must be the case for the tensile resultant in the central line (for symmetry reasons). This is not so clear for the tensile and compressive resultants on the corner lines. Nevertheless, these resultants are close to horizontal if the displacements of the plates are small with respect to the dimensions of the slab.*

When the resultant forces are calculated as a function of the maximum forces that exist at the extremities of the corner lines, the expression mentioned previously allows computing a parameter  $k$  which is the ratio between the compressive membrane force in the corner lines (i.e., at the corners of the slab) and the tensile force at the other extremity of the corner lines (points A on Figure 4).

The next step is the derivation of the maximum tensile force at this extremity of the corner line where it meets the central line. Two possibilities are considered, each one associated with a failure mode.

- 1) The first failure mode is a tensile crack in the center of the slab, parallel to the short edge of the slab (line EF on Figure 6). It is assumed that this crack extends from one to the other longitudinal edge of the slab, which implies that the compressive zone near the long end of the slab (point E) has a width that is infinitely small. The tensile force along the crack is calculated assuming that all the reinforcement along the section is at ultimate tensile strength.

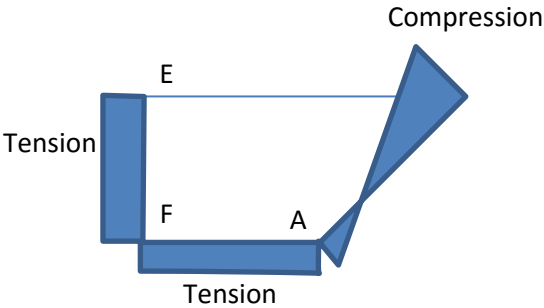


Figure 6: membrane forces in failure mode 1

The equilibrium of moment of the resultants with respect to point E yields the parameter  $b$  which defines the tensile force at point A.

Notes:

- 1) In the equilibrium of moment mentioned above, the shear force  $S$  along the corner line is taken into account. The value of this shear force is calculated from horizontal equilibrium of the triangular plates, see Figure 7.
- 2) If the horizontal component of the shear force and the horizontal component of membrane forces are in equilibrium on the corner line in the triangular plate, see Figure 7, they are also in equilibrium in half the plate of Figure 6. As a consequence, the plate shown on Figure 6 is in horizontal equilibrium only if the compressive force that is concentrated on point E is equal to the horizontal tensile force on line EF.

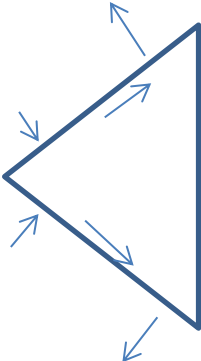


Figure 7: triangular plate

- 2) The second failure mode is compressive failure of concrete in the corners of the slab. The total compressive force in the section is the addition of:
  - a. the compressive membrane force that can be seen on Figure 4 and
  - b. the compressive force due to the bending along the yield line.

The total of these two forces cannot yield a compressive stress that exceed  $0,85 \times f_{ck}$  calculated on the hypothesis that the maximum stress-block depth is equal to  $0,45 d$ . This value of  $0,45$  is a very strong hypothesis that the authors of the method don't justify.

The fact that two different enhancement factors are obtained for the trapezoidal and the triangular plates would be due, according to Tony Gillies, to the fact that the vertical shear component between the trapezoidal and the triangular plates (i.e. in the corner yield lines) has been neglected in the equilibrium equations.

### 1.2.2 The enhancement factor

Now, assuming that we have all membrane forces inside the element and that they are correctly evaluated, here are some thoughts about the enhancement factors.

We will use a uniaxial element, in order to simplify the discussion. We assume that the element is supporting a UDL of value  $p$ . The span is  $L$ .

#### 1) Simply supported beam, no axial force, no large displacement

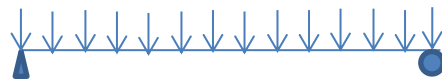


Figure 8: simply supported beam

Acting bending moment at mid spa:  $M = pL^2/8$

Acting axial force:  $N = 0$

Bending capacity of the section:  $M_{pl} = W_{pl} f_y$

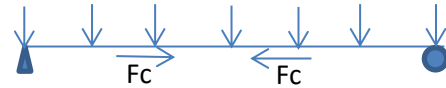
The ultimate load is given by  $p_0 = 8 M_{pl} / L^2$

This corresponds to Eq. (5.2) in the ECCS publication.

This is called the reference plastic load. This is the one that we have to enhance.

## 2) Simply supported beam, with an axial force, no large displacement

Let us assume now that, for any reason, the central part of the beam is subjected to a compressive force  $F_c$  in addition to the applied vertical loads. There is still no large displacement considered.



Acting bending moment at mid spa:  $M = pL^2/8$

Acting axial force:  $N = F_c$

If the section is made of reinforced concrete, the compressive axial force will increase the resisting bending capacity of the section, Figure 9, see Eq. (5.34) in ECCS publication.

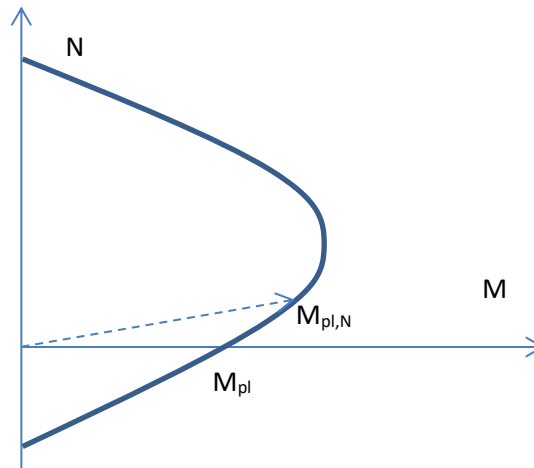


Figure 9: M-N interaction diagram

The ultimate value of  $p$  is now given by:

$$P = 8 M_{pl,N} / L^2$$

If we note  $e_2$  the ratio  $M_{pl,N}/M_{pl}$ , we can write  $p = e_2 p_0$

Note that, if the axial force is tension,  $e_2$  could be smaller than 1. It is then amazing that the *overall* factor  $e_2$  calculated for the biaxial slab panel treated by the Bailey-Moore method is greater than one, since most of the member is subjected to tensile forces. In fact, as there is no horizontal force applied on the slab panel as a whole, tensile and compressive forces equilibrate each other in the slab panel and, indeed, application examples carried out systematically yield a value of  $e_2$  that is very close to 1,0.

### 3) Deformed beam with an axial force, no enhancement of the plastic resistance

Let us assume now that the beam is still supporting vertical loads but is also subjected to large displacement of amplitude  $w$  and a tension horizontal reaction  $F_t$ , see Figure 10. Let us assume also that the section is such that the bending resistance is not influenced by the axial force. This may happen, for example, if the section is made of steel and the axial force is small.

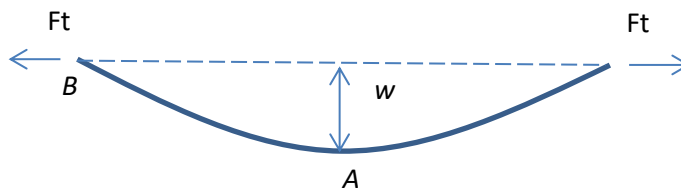


Figure 10: uniaxial member with a horizontal force

Acting bending moment at mid spa:  $M = pL^2/8 - F_t w$

Acting axial force:  $N = - F_t$

The ultimate value of  $p$  is now given by:  $p = 8 (M_{pl} + F_t w) / L^2$

If we note  $F_t w / M_{pl} = e_1$ , we can write  $p = p_0 (1+e_1)$

We see that  $e_1$  is proportional to the displacement  $w$ .

Note that, in a uniaxial element that deflects downward, we need a tensile reaction force at the support to decrease the bending moment at mid span. In a biaxial element, we have tension in the center as well as compression forces near the supports which are in self equilibrium.

It is somehow amazing to note that the moment produced by the axial forces is evaluated in the Bayley-Moore method, for each rigid plate, with respect to the supports.

Indeed, the effects of actions (bending moment and axial force) must be evaluated and checked, normally in any section, practically in the most critical section(s), here along the yield lines and not along the supports where no effect of action is present.

For example, in the uniaxial situation like the one shown in Figure 10, the critical section is section A located at mid span. The effects of action ( $M^A$ ,  $N^A$ ,  $V^A$ ) can be easily calculated from the equilibrium of half a section, see Figure 11, assuming that we know the value of the horizontal reaction  $F_t^B$  (the uniformly distributed load  $p$  has not been represented on this figure for clarity reasons).

The shear force  $V^A$  is equal to 0, because the vertical reaction  $R^B$  balances exactly the vertical load  $pL/2$  applied on this substructure.

The axial force  $N^A$ , that we will call here  $F_t^A$  is exactly equal to the horizontal reaction  $F_t^B$  from the equilibrium in the horizontal direction.

The bending moment  $M^A$  has contributions from the vertical forces and a contribution from horizontal forces.

$$M^A = M^A(\text{vertical forces}) + M^A(\text{horizontal forces})$$

$$= [ pL/2 \times L/2 - pL/2 \times L/4 ] - F_t^B \times w^A$$

$$= pL^2/8 - F_t^B \times w^A$$

We can nevertheless verify that the same result is obtained for the contribution of the horizontal forces if the moment is evaluated with respect to the support, point B, see Figure 11. Indeed:

$$M_B = F_t^A \times w^B = M_A = F_t^B \times w^A$$

Because  $F_t^A = F_t^B$  and  $w^B = w^A$

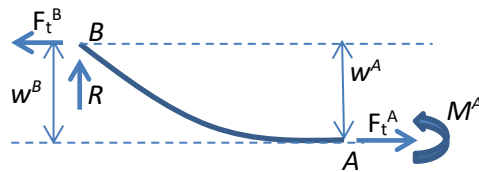


Figure 11: half of the uniaxial member with a horizontal force

It can be noted that the same equivalence holds for vertical forces because the moment of vertical forces with respect to point B is  $pL/2 \times 0 + pL/2 \times L/4 = pL^2/8$

This is because of a principle of structural mechanics: when a group of forces is in equilibrium in translation, if they produce a certain moment with respect to a point in the plane, they produce the same moment with respect to *any* point in the plane.

In the biaxial situation that prevails in a slab panel, the critical sections are along the yield lines. The same principle can be generalized: when a group of forces is in equilibrium in translation, if they produce a certain moment with respect to an axis in space, they produce the same moment with respect to any parallel axis in space.

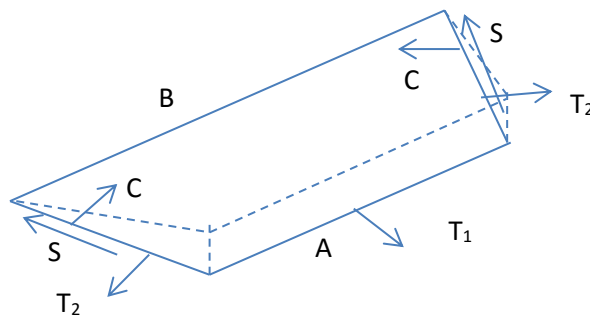


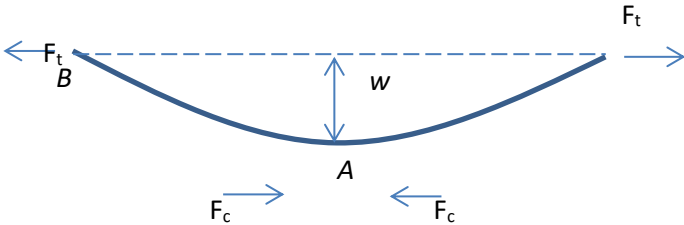
Figure 12: bending moment with respect to the support

For the trapezoidal plates such as the one shown on Figure 12, taking the moments produced by membrane forces S, T<sub>1</sub>, T<sub>2</sub> and C with respect to the axis B on the support is thus equivalent to evaluating the moments with respect to the central yield line A because these forces are in equilibrium in translation. In the simple method, this contribution is divided by the plastic capacity of the slab M<sub>p1</sub> (in Nm/m) multiplied, not by the length of this yield line but by the length of the slab in the longest direction L. Maybe is this to account for the projection of the bending capacity of the slab in the two corner yield lines on the central yield line.

For the contribution of membrane forces to the reduction of bending moments in the corner lines of the triangular plates, the moment produced by membrane forces  $S$ ,  $T_2$  and  $C$  is also evaluated with respect to the support (now on the short side) and also compared with the plastic capacity in the slab, multiplied now by the length of the short side.

**4) Deformed beam with an axial force and enhancement of the plastic resistance**

We add now the two effects mentioned under point 2 and 3. We have a horizontal reaction near the supports that will decrease the bending moment at mid span (in a biaxial situation, this would be produced by the anchorage of the steel mesh in the outer compression ring). Let us assume that, from the particular statics of bi-axial members, we have at the same time compressive axial forces at mid span that increase the bending strength of the section<sup>5</sup>.



We have now the equation:  $p L^2 / 8 - F_t w = M_{pl,N}$

or,  $(p L^2 / 8) / M_{pl} = e_1 + e_2$

and finally:  $p = p_0 (e_1(w) + e_2)$

which is Eq. (5.49) of the ECCS publication.

This simple reasoning explains why the two enhancement effects really add to each other whereas intuition would lead to multiply two enhancement factors. The fact that the two enhancement factors must be added and that the sum multiplies the yield line ultimate load, see the equation above, can also be accepted more easily when one notes that, if the enhancement is small,  $e_1$  tends toward 0 and  $e_2$  tends toward 1.

<sup>5</sup> If the force is tension, it will decrease the bending resistance

### 1.2.3 Estimation of the displacement

The displacement in the center of the slab is a key parameter of the method because it influences strongly the enhancement factor. This displacement must be estimated.

In the simple method, this displacement is made of two components: one due to thermal bowing assumed to be given by a circular deformed shape and one due to elongation of the bars from applied stresses assumed to be given by a parabolic shape.

The fact that both shapes are different is not an issue if the displacements can be added. The fact that the thermal bowing is calculated based on the short span whereas the mechanical displacement is based on the long span may lead to think of a system where two elements are working in parallel (more or less as one beam across the short span and another beam across the long span, both having the same displacement in the center of the slab) and their respective displacements are added. In fact, the model does not say so. The model admits that there is a thermal displacement and a mechanical displacement in each direction. More difficult to explain are the facts that:

- 1) Each displacement is evaluated based on a uniaxial behavior, as if there is no effect from the other direction.
- 2) The thermal displacement is based on the short span (probably the best choice if it has been decided to consider a uniaxial behavior) but the mechanical displacement is based on the long span whereas consideration of the short span is expected to give the true behavior if the aspect ratio (long span/short span) tends to high values.
- 3) These continuously derivable shapes considered here are totally incompatible with the multilinear shapes considered in the yield line theory which is at the base of the method, see Figure 13.

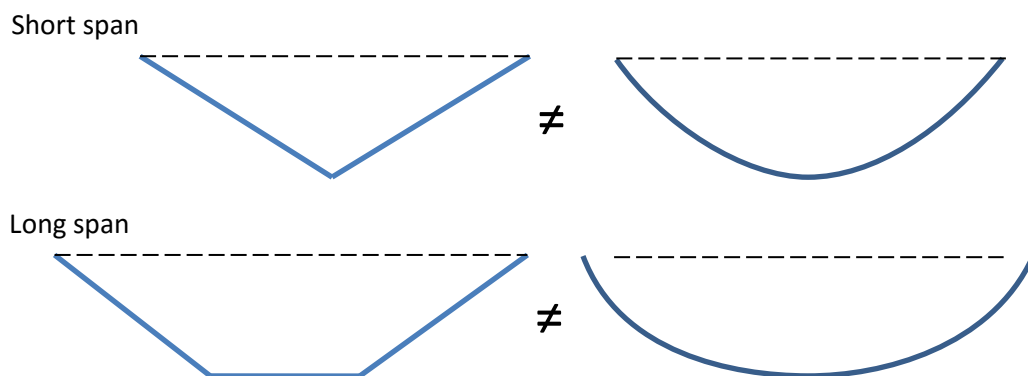


Figure 13: non compatible displacement modes

### 1.2.4 Contribution of the unprotected beams

In the simple method, the load bearing capacity of the unprotected beams is taken as the bending capacity of the composite beams made of the unprotected steel profiles collaborating with the concrete slab. This means that the upper part of the concrete slab is assumed to work here in compression at mid span of the beams, i.e. in the center of the slab where, for the evaluation of the membrane forces, the slab is assumed to be fully cracked in tension. This is a severe contradiction.

The contribution of the unprotected steel beams to the loadbearing capacity is particularly significant during the first 30 minutes of the fire and decreases thereafter with the elevation of temperature in the unprotected steel sections. The contribution of the unprotected steel beams may nevertheless still account to around 15% of the contribution of the slab, even after 2 hours of ISO fire.

### 1.3 The FRACOF method

The method has first been evaluated from its implementation in the software MACS<sup>+</sup>, version 3.0.1, August 2013.

The input data can be given in a user friendly graphical interface. This interface can be set to have the text in 16 different languages.

If the user tries to introduce any value that is beyond the field of application of the software, it is impossible to proceed further. The user is forced to change the value to continue the input of data.

Once entered in the graphic interface, the input data can be saved in a file with extension “.frc”. This file is a text file organized according to an XML format and can thus be opened by a text editor. A series of input files can thus also be generated by any convenient mean, for example to run parametric analyses.

As far as we could observe, the software is quite robust (it does not crash during execution or from any action of the user) and the implementation of the Bailey-Moore method is correct<sup>6</sup>.

It is also quite easy to use. It has been verified, for example, that there is a sketch showing the definition of the longitudinal mesh area as opposed to the transverse mesh area. The sketch is in the screen “Slab”, see Figure 14. The longitudinal bars are parallel to the span 1, i.e. parallel to the internal unprotected beams.

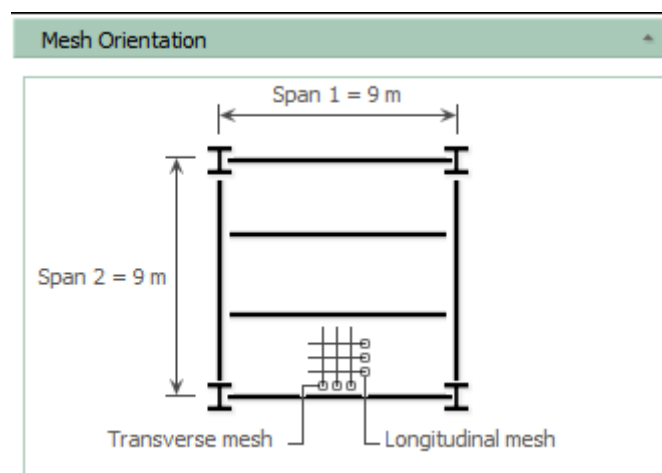


Figure 14: orientation of the mesh

The reinforcement mesh is assumed to be made of cold-formed steel (private communication). Since version 3.01, it is possible to consider flat slabs (in addition to corrugated slabs).

<sup>6</sup> A complete and full verification could of course not be performed within the frame of this study.

Limitations of the software:

- It is not possible to evaluate the fire resistance of a slab panel that has no unprotected beam. At least one unprotected beam must be present. This is yet not surprising as the aim of the software is to check the stability of slab panels with internal unprotected beams. It is nevertheless still possible to approach the solution with no unprotected beams by introducing a single beam with a minimal section and minimal yield strength.
- The beams that form the slab panel must be based on hot rolled steel profiles, either used as such or in the form of cellular beams (beams with large web openings), either based on European, UK, or American sections. It is not possible to define user (welded) sections.
- European sections must be of the IPE type.

Other limitations apply, normally conforming to common sense and documented in the ECCS publication and/or in the contextual help of the software. The contextual help comes in the form of short text appearing in a window called “messages”, depending on the position of the cursor in the input boxes.

In addition to a list of input data, the results produced in the report are, at a constant time step that varies between 1 and 10 minutes depending on the requested fire duration, see Figure 15:

- The temperatures of the unprotected beam, of the mesh, at the top and at the bottom of the slab (the software does not warn if the insulation criteria I is lost on top of the slab);
- The beam capacity in kN/m<sup>2</sup>, decreasing as a function of time as the temperature in the beam increases;
- A deflection that is, unduly in our opinion, called “maximum allowable deflection”. We rather consider this value,  $w$  in the theory, as an intermediate result, a parameter that is evaluated to lead to the final result. This value usually increases as a function of time;
- The ultimate load bearing capacity of the slab according to the yield line theory (without enhancement owing to membrane effects). This value reduces as a function of time as the temperature of the mesh increases;
- The enhancement factor. It typically increases first because of the rapid increase of the displacement but may decrease slightly later when the displacement has reached a constant value;
- The slab capacity taking into account the enhancement factor (product of the two previous values);
- The total capacity, sum of the beam capacity and the slab capacity;
- The unity factor, ratio between the applied load and the total capacity. The fire resistance time is met when this factor is 1.

The software does not give information about the contribution of both components of the enhancement factor  $e_1$  and  $e_2$ . There is also no information about the failure mode, by tension in the steel mesh or by compression in the concrete slab.

We have not seen how it could be possible to save in a pdf file the report that contains the data and the results.

Time	Beam	Mesh	Slab top	Slab bottom	Beam capacity	Maximum allowable deflection	Slab yield	Enhancement	Slab capacity	Total capacity	Unity factor
mins	°C	°C	°C	°C	kN/m <sup>2</sup>	mm	kN/m <sup>2</sup>		kN/m <sup>2</sup>	kN/m <sup>2</sup>	
0	20	20	20	20	22.62	233	2.65	1.68	4.46	27.08	0.25
10	304	39	21	365	22.57	327	2.65	1.96	5.20	27.78	0.25
20	641	67	28	600	7.03	389	2.65	2.15	5.70	12.73	0.54
30	802	117	41	718	2.50	417	2.65	2.23	5.92	8.43	0.81
40	867	164	59	791	1.80	432	2.65	2.28	6.04	7.85	0.87
50	907	185	73	843	1.41	442	2.65	2.31	6.13	7.53	0.91
60	937	222	87	883	1.27	449	2.65	2.33	6.18	7.44	0.92
70	962	259	90	915	1.15	457	2.65	2.35	6.24	7.39	0.93
80	983	291	105	941	1.05	460	2.65	2.36	6.27	7.31	0.94
90	1001	321	118	964	0.96	463	2.62	2.37	6.21	7.17	0.95
100	1018	349	138	984	0.88	463	2.58	2.36	6.11	6.99	0.98
110	1032	375	155	1001	0.81	463	2.55	2.36	6.02	6.83	1.00
120	1046	399	168	1017	0.74	464	2.51	2.36	5.94	6.68	1.02
130	1058	420	180	1031	0.68	464	2.38	2.36	5.61	6.29	1.09
140	1070	440	191	1044	0.63	465	2.25	2.35	5.28	5.91	1.16
150	1080	458	201	1056	0.58	465	2.13	2.34	4.99	5.57	1.23
160	1090	475	210	1067	0.53	466	2.02	2.34	4.72	5.25	1.30
170	1099	490	218	1078	0.49	467	1.91	2.34	4.46	4.95	1.38
180	1108	505	225	1088	0.44	468	1.81	2.33	4.23	4.68	1.46

Figure 15: results produced by MACS+

The load has to be introduced by the values of the leading variable action, the accompanying variable action, the dead load including beam (excluding slab) and the slab weight including mesh (this one can be automatically calculated by the software based on the steel sheet dimensions or can be entered by the user). The partial safety factors in the fire situation must also be entered for the leading variable action of for the other variable action. The partial safety factor for permanent action is fixed to 1. The design load in case of fire that results from these values is given in the report. It can be verified on Figure 16, for example, that  $(1,25 + 2,825) \times 1,0 + 5 \times 0,5 = 6,575 \text{ kN/m}^2$  has been correctly applied (we introduced the slab weight directly).

6. Loading details	
• Normal (Cold)	
Leading variable action:	5 kN/m <sup>2</sup>
Accompanying variable action:	0 kN/m <sup>2</sup>
Dead load including beam, excluding slab:	1.25 kN/m <sup>2</sup>
Slab weight including mesh:	2.825 kN/m <sup>2</sup>
• Fire (Hot)	
Combination factor for permanent action:	1.0
Combination factor for leading variable action:	0.5
Combination factor for other variable action:	0.3
7. Fire & Analysis	
• Standard temperature-time curve	
Fire resistance period:	60 min
8. Summary output	
• Default mesh direction	
Maximum unity factor:	1.66 <b>Floor slab fails</b>
Factored load in fire:	6.58 kN/m <sup>2</sup>
Fire curve:	Standard temperature-time curve

Figure 16: input of loads (correct)

Yet, for other cases, we get erratic results, see Figure 17. This was due to the utilization of a coma instead of a decimal point as a decimal separator. As shown by the difference in maximum unity factor and in the message (“Floor slab adequate” or “Floor slab fails”), the software really considers the factored load that appears in the summary output to check the stability of the composite slab. If this value is wrong because of the utilization of the wrong decimal separator, the result of the calculation will be wrong.

6. Loading details		6. Loading details	
• Normal (Cold)		• Normal (Cold)	
Leading variable action:	5 kN/m <sup>2</sup>	Leading variable action:	5 kN/m <sup>2</sup>
Accompanying variable action:	0 kN/m <sup>2</sup>	Accompanying variable action:	0 kN/m <sup>2</sup>
Dead load including beam, excluding slab:	1,25 kN/m <sup>2</sup>	Dead load including beam, excluding slab:	1,25 kN/m <sup>2</sup>
Slab weight including mesh:	2,825 kN/m <sup>2</sup>	Slab weight including mesh:	2,825 kN/m <sup>2</sup>
• Fire (Hot)		• Fire (Hot)	
Combination factor for permanent action:	1.0	Combination factor for permanent action:	1.0
Combination factor for leading variable action:	0,5	Combination factor for leading variable action:	0.5
Combination factor for other variable action:	0,3	Combination factor for other variable action:	0.3
7. Fire & Analysis		7. Fire & Analysis	
• Standard temperature-time curve		• Standard temperature-time curve	
Fire resistance period:	120 min	Fire resistance period:	120 min
8. Summary output		8. Summary output	
• Default mesh direction		• Default mesh direction	
Maximum unity factor:	0.69 <b>Floor slab adequate</b>	Maximum unity factor:	1.26 <b>Floor slab fails</b>
Factored load in fire:	3 kN/m <sup>2</sup>	Factored load in fire:	5.5 kN/m <sup>2</sup>
Fire curve:	Standard temperature-time curve	Fire curve:	Standard temperature-time curve

Figure 17: input of loads (incorrect)

After we mentioned this to CTICM, we received by private e-mail dated 16/11/2015 the version 3.0.2 of MACS in which this problem has been solved. Nevertheless, on 30/05/2016, version available for download on the web site of ArcelorMittal was still version 3.0.1.

We did not check the effects of using a wrong decimal separator in other entries of the software.

## 2 Numerical simulations

According to the request of CERIB, the method that will be analyzed here is Bailey-Moore simple method applied to composite floors based on trapezoidal or reentrant cold formed steel decks. The composite floor is supported by steel beams with at least one unprotected steel beam in a slab panel. The floor acts in a composite manner with the steel beams.

The simple method is evaluated by its implementation in the software MACS<sup>+</sup> developed by CTICM and ArcelorMittal. It is evaluated by comparison with results obtained by the general calculation model.

The numerical analyses have been performed by the software SAFIR<sup>®</sup>, version 2016.b.1. In the numerical simulations, a physical reason was found at the end of nearly all runs, either a vertical asymptote in the displacement curve, or steel entering in the descending branch in either the steel beam or at least one shell finite element.

### 2.1 Thermal simulations

Only the ISO 834 fire curve is considered in this analysis.

#### 2.1.1 Model of the composite slab

Thermal properties of concrete are from the Eurocodes, with specific mass of 2300 kg/m<sup>3</sup>, water content of 46 kg/m<sup>3</sup> (2%), coefficient of convection on exposed surface of 25 W/m<sup>2</sup>K, coefficient of convection on unexposed surfaces of 4 W/m<sup>2</sup>K, emissivity of 0,7 and thermal conductivity equal to the average between lower limit and upper limit as defined in clause 3.3.3 (2) of EN 1992-1-2.

As the shell finite element of SAFIR is a flat element, the section of the composite floor is simplified. The presence of the steel deck is not taken into account, neither in the thermal nor in the structural analyses (this hypothesis is also taken into account in MACS<sup>+</sup>).

The concrete slab located above the steel deck is modeled with its exact depth while the ribs of the slab are modeled by a smeared uniform layer of concrete (this protective layer will have no load bearing capacity in the structural analysis).

In order to choose the appropriate value for the thickness of the protective layer, a model has first been made of a real 2D section. We modeled in SAFIR the COFRA+60 composite slab. The steel deck is not modelled and no shadow effect is considered. We can see that the temperature at the level of the mesh is not uniform, see Figure 18.

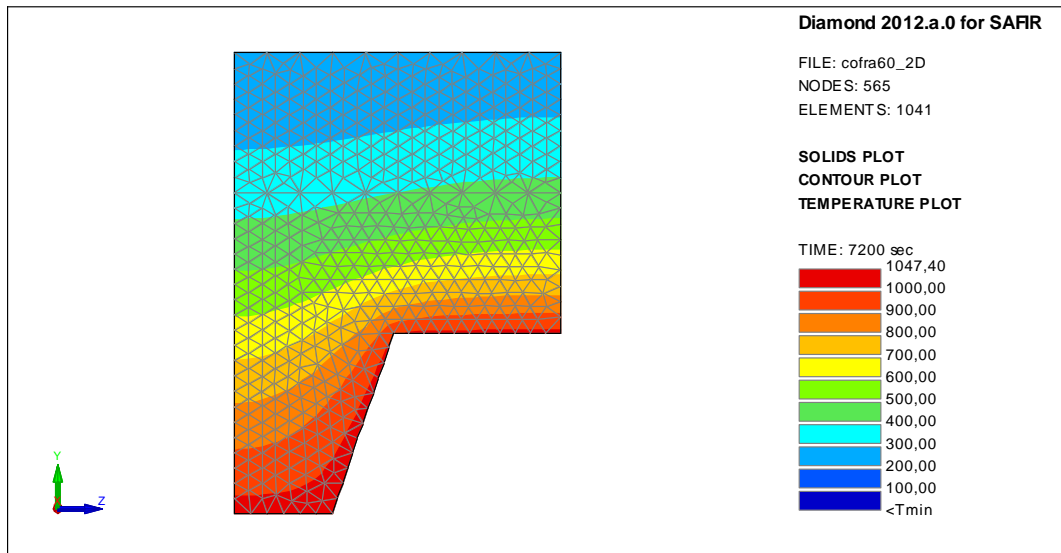


Figure 18: isotherms after 120 minutes

We noted the evolution of the temperature at the level of the steel mesh for 3 points in the model of Figure 18: extreme left, extreme right and intermediate position. This evolution is shown in Figure 19 together with the temperature evolution given by MACS+. It can be seen that MACS+ follows more or less the temperature calculated by SAFIR for the intermediate position<sup>7</sup> during 30 minutes and is closer to the maximum temperature thereafter. The hypothesis used in MACS+ thus seems to be reasonable, even slightly on the safe side compared to the results given by SAFIR.

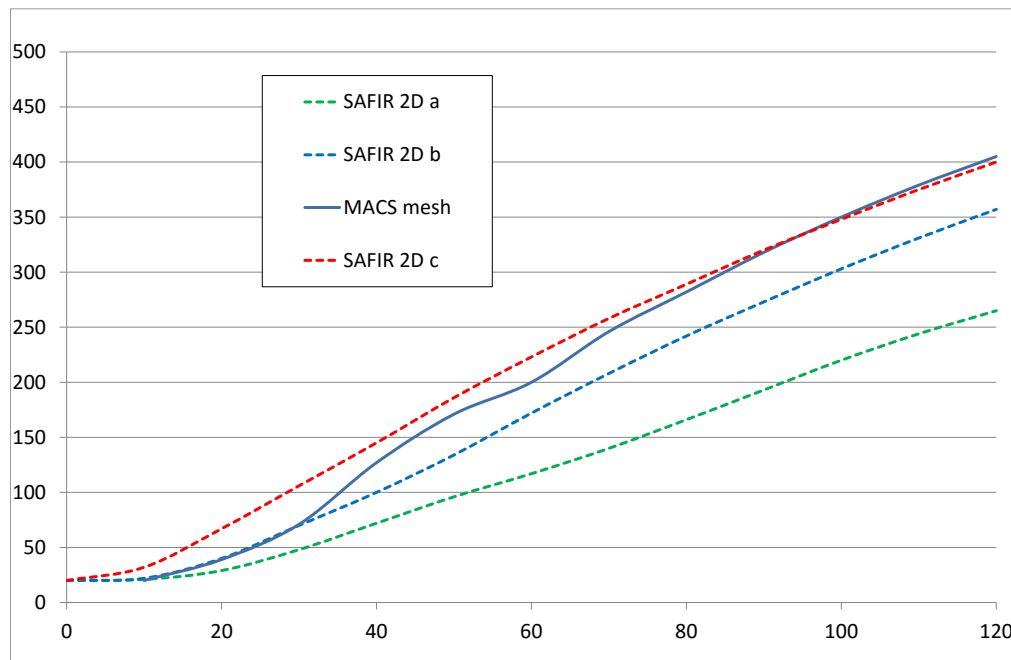


Figure 19: evolution of the temperature in the steel mesh

<sup>7</sup> This temperature can be assimilated to the average temperature in the steel mesh.

In order to derive the thickness of the protective layer for the flat slab model, equation D.15 of EN 1994-1-2 was first used. We considered a COFRA+ 60 section with 90 mm of concrete on top; equation D.15 gives an equivalent thickness of the slab equal to 23 mm; we thus made a flat slab model with a total thickness equal to 113 mm. There is not a very good fit between SAFIR and MACS+ for the temperatures at the level of the mesh, see Figure 20. It has to be noted that equation D.15 has been derived to yield good fit with the temperature on the unexposed side of the composite floor, with the Insulation criteria *I* in mind, see how the curves “MACS top” and “SAFIR top” compare well on Figure 20.

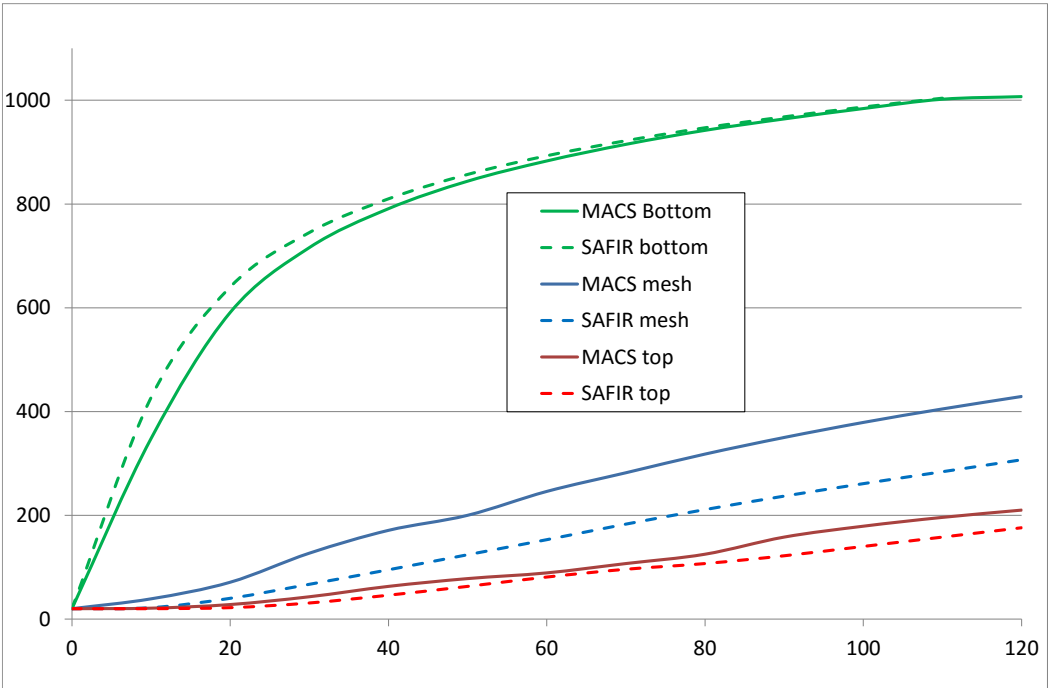


Figure 20: comparison between SAFIR 1D and MACS+ in a COFRA+ 60 with 23 mm protective layer

Yet, in tensile membrane action, the temperature on the unexposed side is not likely to dominate the failure mode. The temperature at the level of the mesh is more likely to be the relevant parameter. This is why different models have been created until a good fit is observed with the temperature at the level of the mesh supposed to be located at mid-depth of the concrete layer, i.e. 45 mm above the steel deck and 45 mm below the surface of the concrete slab. A protective layer of 5 mm was finally chosen. Figure 21 shows the good comparison obtained at the level of the mesh as well as on the exposed side of the slab. The temperatures on the unexposed side are overestimated by 30°C after 60 minutes while still remaining so low that this should not affect the failure mode by compression in the concrete.

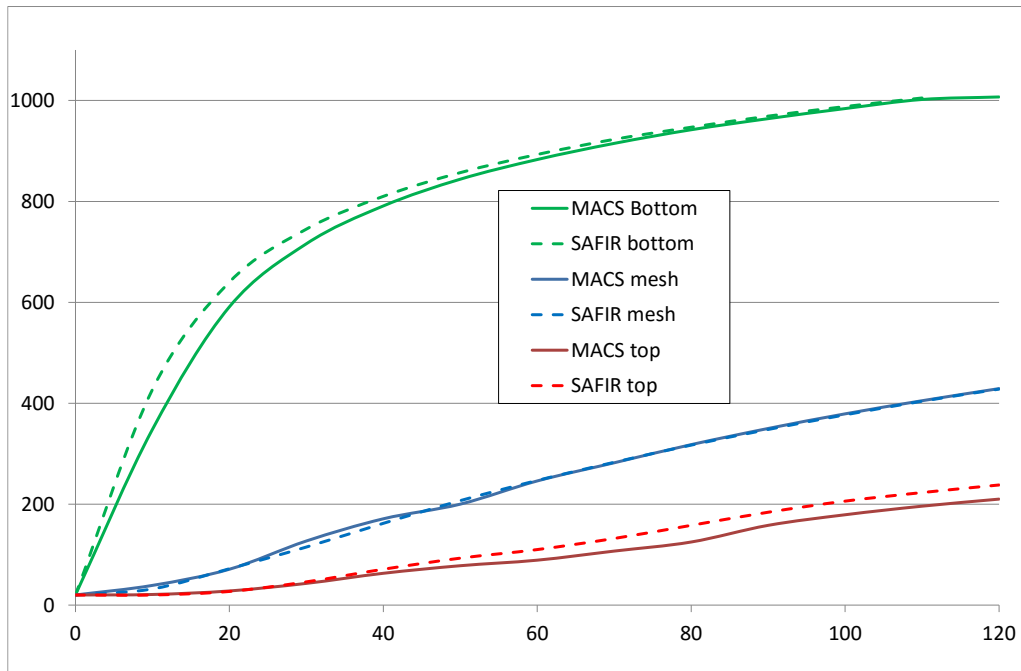


Figure 21: comparison between SAFIR 1D and MACS+ in a COFRA+ 60 with 5 mm protective layer

As a conclusion of this section, we note that:

- 1) MACS+ seems to give a correct (slightly on the safe side) estimation of the temperature in the steel mesh compared to the results of a SAFIR 2D numerical model.
- 2) When a flat slab is used with an equivalent horizontal layer of concrete representing the protective effect of the ribs, it is better in the numerical model to reduce the thickness of this layer compared to the value given by equation D.15 of EN 1994-1-2 if a correct evaluation of the temperature at the level of the steel mesh is the objective.

### 2.1.2 Model of the steel beams

The steel beam has the upper flange somehow protected by the composite slab. Nevertheless, as the proportion of the upper flange covered by the steel deck is less than 90% (when the deck is a COFRA+ 60), the steel profile is heated on 4 sides in the simulations.

For IPE 360, the coefficient of convection and the emissivity of steel are multiplied by the factor  $0,9 \times 2 \times (0,36 + 0,17) / 1,353 = 0,705$  in order to introduce in the numerical model the shadow effect<sup>8</sup>.

- ⇒ Coefficient of convection;  $0,705 \times 25 = 17,63$
- ⇒ Emissivity:  $0,705 \times 0,7 = 0,4935$

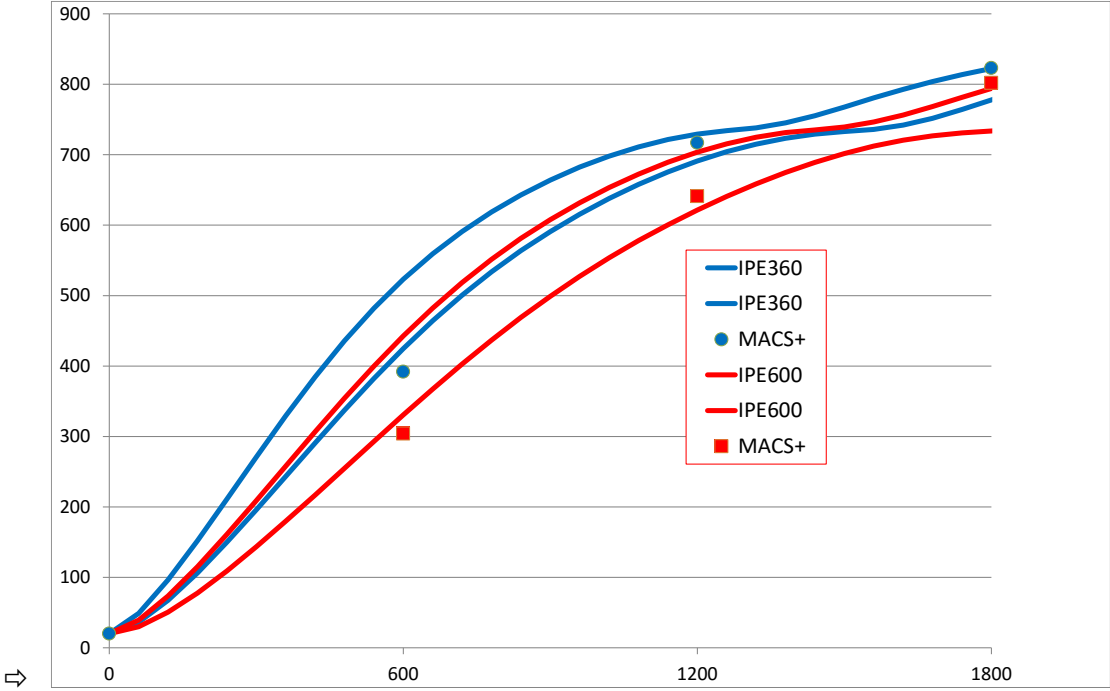
For IPE 600, for example, the coefficients are multiplied by  $0,9 \times 2 \times (0,60 + 0,22) / 2,015 = 0,733$

- ⇒ Coefficient of convection;  $0,733 \times 25 = 18,33$
- ⇒ Emissivity:  $0,733 \times 0,7 = 0,5131$

Figure 22 shows the evolution in two steel beams, IPE360 in blue and IPE600 in red, as calculated by SAFIR (minimum and maximum temperature in the section) and by MACS+ (results given every 10

<sup>8</sup> See EN 1993-1-2

minutes). It can be seen that the temperatures are slightly lower in MACS+ during the first 15 minutes but this is not considered to be a serious issue because no slab panel is designed for a 15 minutes resistance time. Between 15 and 30 minutes, the temperatures calculated by MACS are between the minimum and the maximum value given by SAFIR. Beyond 30 minutes, the temperatures calculated by MACS+ rather correspond to the maximum values calculated by SAFIR, with little differences between all values because steel temperatures tend toward the values of the ISO curve.



⇒ Figure 22: Evolution of the temperature in steel beams

As a conclusion of this section, we consider that the temperatures in unprotected steel beams are correctly evaluated by MACS+

### 2.1.3 Some results

Here are some typical results obtained by the numerical simulations for steel beams and for concrete slabs.

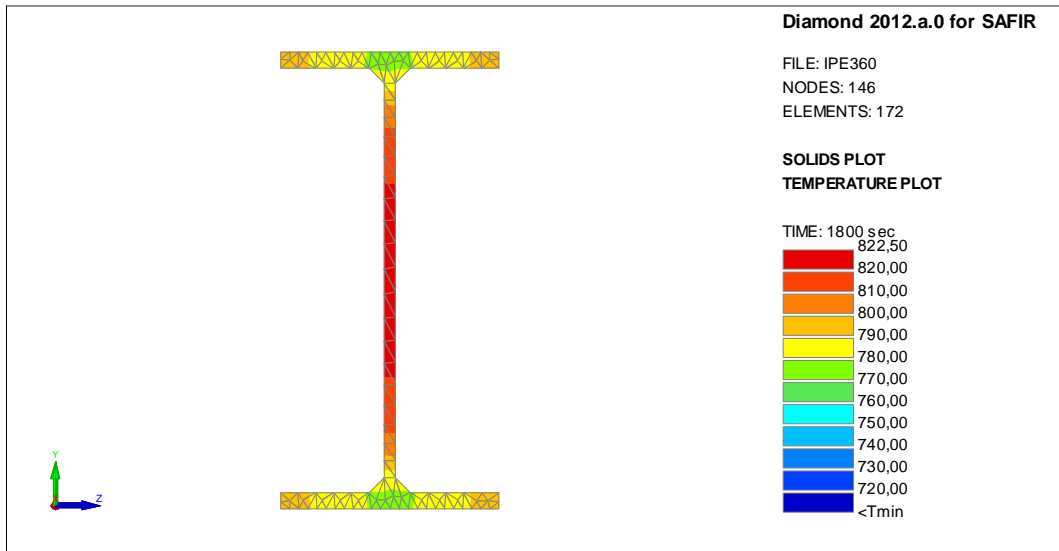


Figure 23: IPE360 heated on 4 sides

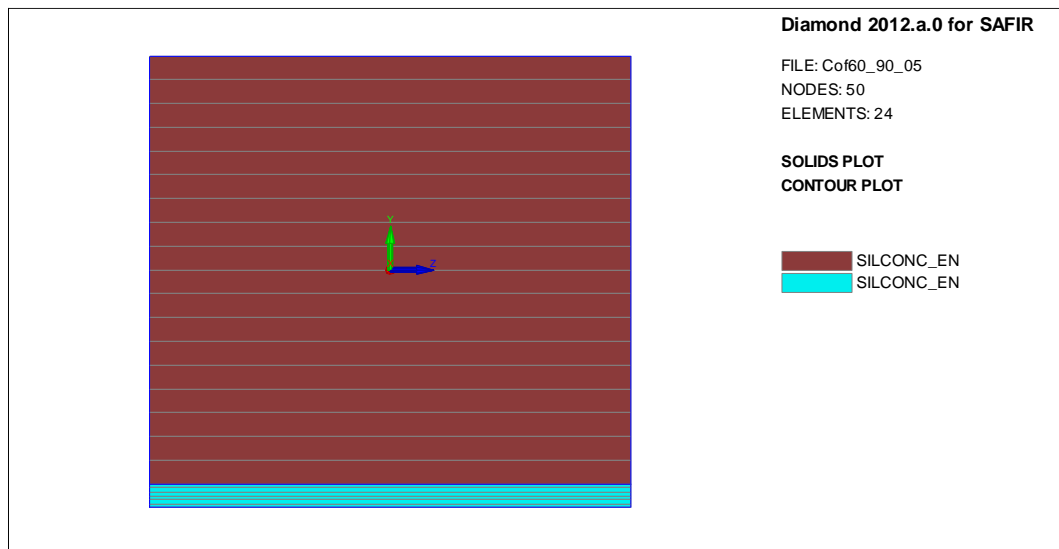


Figure 24: 90 mm slab with 5 mm of insulating concrete – discretisation

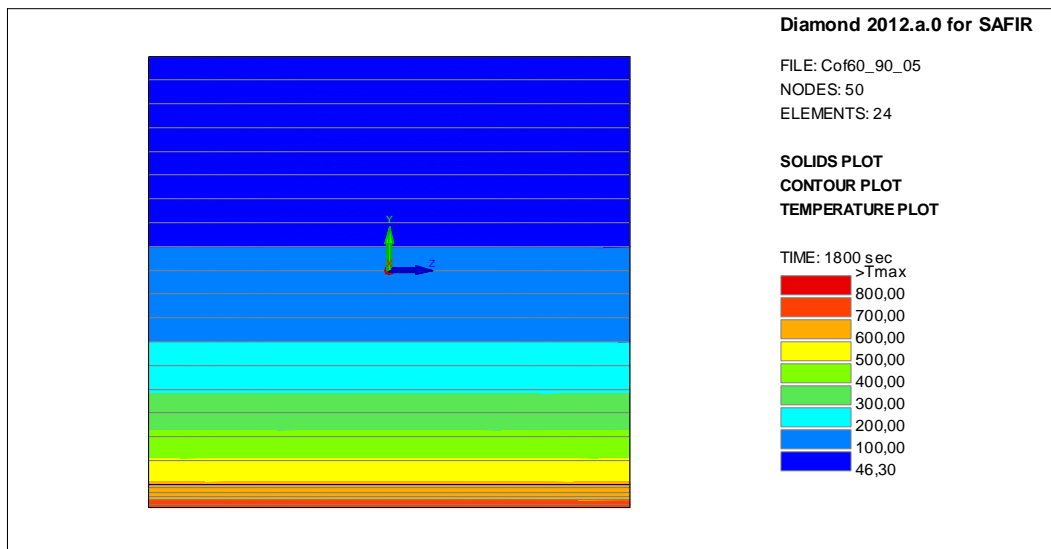


Figure 25: 90 mm concrete slab with 5 mm insulating concrete – isotherms

## 2.2 Mechanical simulations

### 2.2.1 The model

Slab panels are modelled by a combination of 3D Bernoulli beam finite elements and shell finite elements.

- Beam elements are used to represent the unprotected steel beams located *within* the slab panel.
- Shell finite elements are used to model the concrete slab located on the perimeter beams and on the unprotected perimeter beams.
- The beam elements share their end nodes with the nodes of the shells located above the beams which ensures a full composite action between the beams and the slab.
- The level arm between the steel beam and the concrete shell is fully taken into account because the node line of the beam (where the displacements are calculated and the forces are transmitted from element to element) is located at mid-level of the structural part of the concrete slab.

Boundary conditions:

- The perimeter beams are not modelled explicitly. A perfect vertical support is supposed on the perimeter of the slab panel, in accordance with the hypothesis of the FRACOF method.
- No horizontal restraint is provided on the perimeter of the slab panel, in accordance with the hypothesis of the FRACOF method. Only the rigid body movements are prevented to ensure convergence of the model.
- When possible, vertical planes of symmetry are considered and only  $\frac{1}{2}$  or  $\frac{1}{4}$  of the slab is modelled.

Figure 26 shows a general overview of a slab panel where only  $\frac{1}{4}$  is modelled.

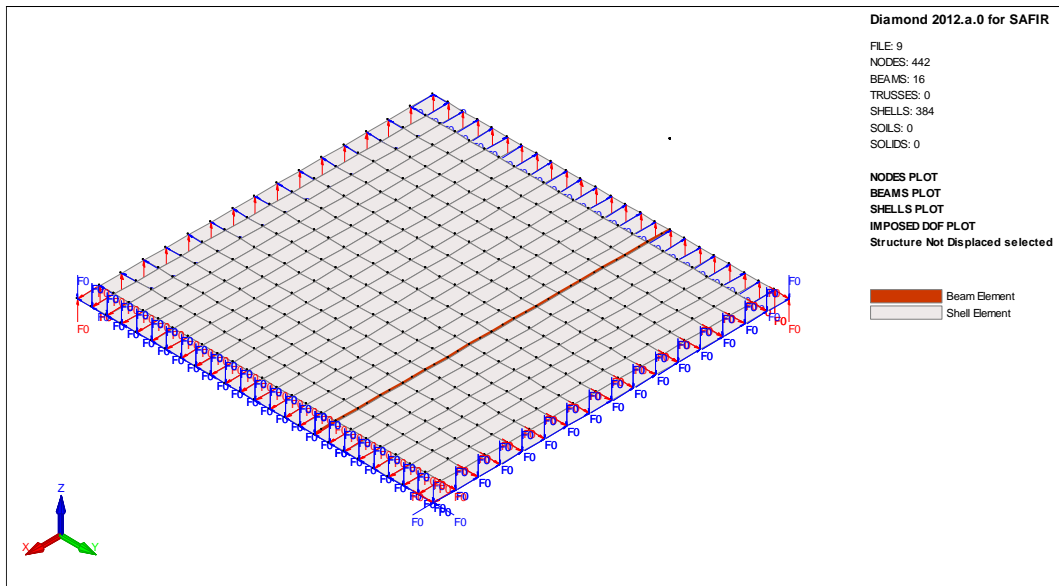


Figure 26: 9 x 9 slab panel with 2 steel beams - 1/4 modelled

Figure 27 shows the boundary conditions on the perimeter of the slab panel: the vertical displacement (in red) and one rotation (in blue) are restrained.

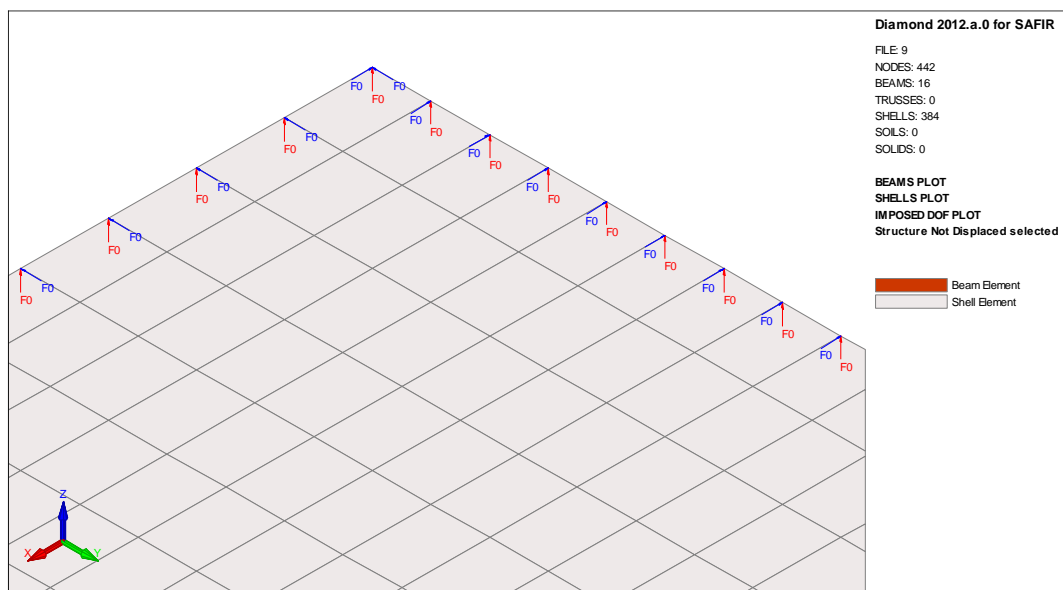


Figure 27: Boundary conditions in the corner of the slab panel

Figure 28 shows the boundary conditions on axes of symmetry of the model: the horizontal displacement perpendicular to the plane of symmetry (in red) and two rotations in the plane of symmetry (in blue) are restrained.

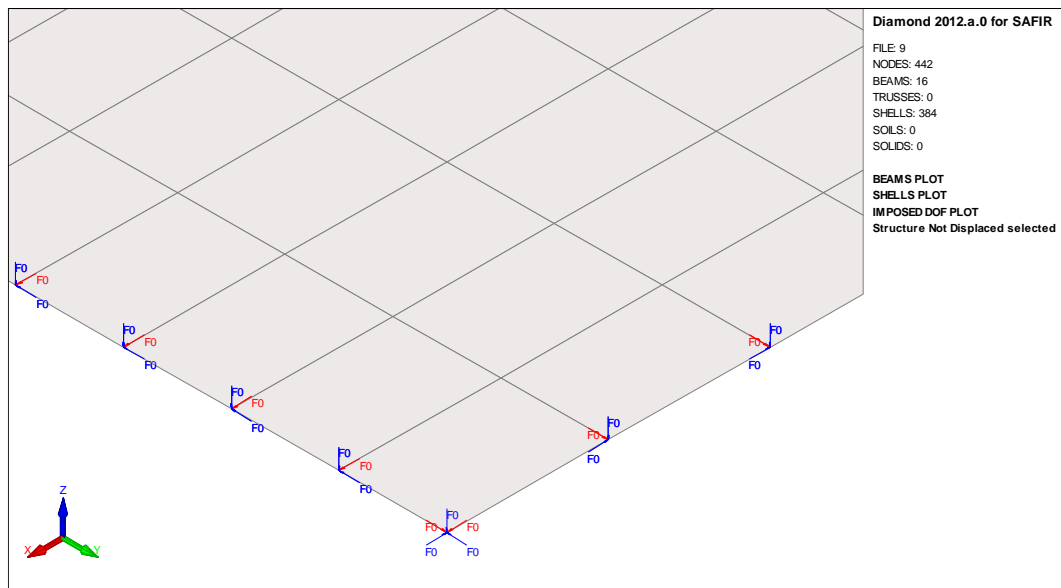


Figure 28: boundary conditions in the center of the slab panel

Compressive strength of concrete is 30 MPa with tensile strength nominally equal to 0 (a value of 0,3 MPa has been used in the models in order to speed up convergence during initial loading). A concrete model that takes transient creep into account explicitly has been considered (Gernay et al, 2013). All models follow Eurocodes recommendations. The composite slab is made of a COFRA+60 trapezoidal sheets. A concrete layer of 90 mm is added on the steel sheets and the ribs are modelled by a 5 mm layer of non-structural concrete. Two layers of reinforcing bars are located at mid-level of the concrete layer (i.e. 45 mm from the top surface) with equal section.

A uniformly distributed load of 6,575 kN/m<sup>2</sup> was applied corresponding to the dead weight of the composite slab (11,3 cm x 25 kN/m<sup>3</sup>), plus a permanent load of 1,25 kN/m<sup>2</sup> + a service load of 0,5 x 5 kN/m<sup>2</sup> (0,5 x 2,5 kN/m<sup>2</sup> for the 9 m x 9 m slab panel, see section 2. 2.4).

Each case was modelled by SAFIR and then calculated by MACS+. In MACS+, full composite action between the steel beams and the composite slab has been considered as in SAFIR.

The quantity of reinforcing bar was varied as a parameter.

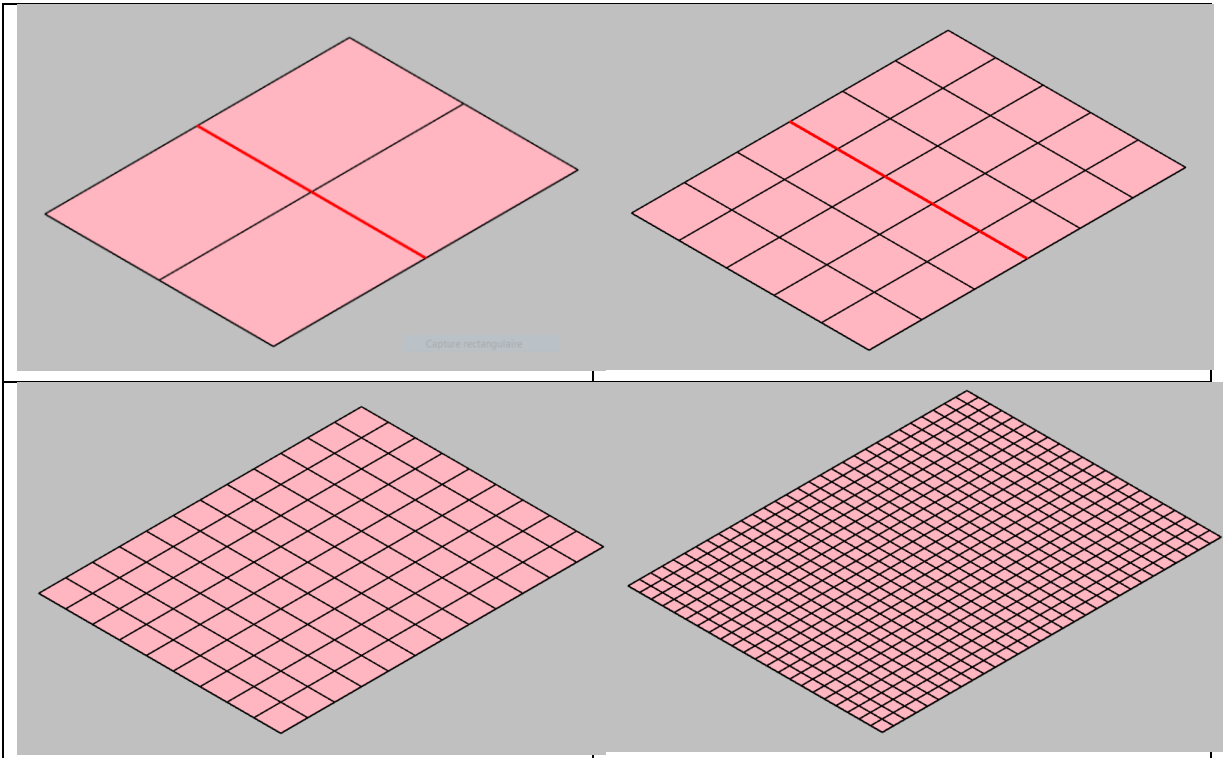
### 2.2.2 Mesh sensitivity

A mesh sensitivity analysis has been performed. It is known that, in elastic problems, the results of displacement type finite elements tend toward the numerical true solution when the size of the elements tends toward 0. A balance has nevertheless to be found between a reasonable precision to be obtained and reasonable computation times.

In order to gain insight into the sensitivity of the size of the elements, a 6 m x 9 m slab panel with 1 IPE 400 has been analyzed. ½ of the panel has been modelled owing to symmetry reasons. The slab contains 200 mm<sup>2</sup>/m of steel in each direction and the total load is 6,58kN/m<sup>2</sup>. The mesh size has

been reduced progressively from 300 cm to 20 cm. Table 1 shows the meshes for elements of 300, 100, 50 and 20 cm.

Table 1: four different meshes



The most important results are reported in Table 2. For this slab panel, the software MACS+ gives a fire resistance time of 40 minutes.

Table 2: results of the mesh sensitivity

Size of the elements	Number of elements	End of Run	$(L+t)/30$	CPU time for 20 minutes of simulation
mm	-	minutes	minutes	seconds
300	4	145	76	58
150	12	136	74	209
100	30	99	67	468
75	48	88	61	828
60	80	91	60	1308
50	108	95	60	2016
38	192	58	55	2949
20	660	44	52	9721

The results are depicted in Figure 29.

It shows a bigger mesh sensitivity when the time of last convergence is considered (EoR) than when a displacement criteria is considered. This shows that, when displacements are excessive, the results of the numerical simulation become less and less reliable. This is because, for excessively large

displacements, the basic hypotheses of numerical simulation (small strains, limited rotations...) are more and more violated. Although the simulation produces some results and numbers, these become more and more meaningless.

The time when the displacement criteria  $(l+L)/30$  is met, on the other hand, is much less sensitive to the refinement of the model. It is amazing that, even with only 4 or 12 elements used to model the structure, a rough estimate can be found with an approximation of only 25%. When the mesh varies from 50 to 75 cm, the result varies by only 1 minute. For smaller meshes, distortion of the slab close to the corners has to be accommodated by one single element in which it is concentrated and slightly earlier failure may occur.

The time needed for a simulation of a certain duration of fire is proportional to the number of finite elements.

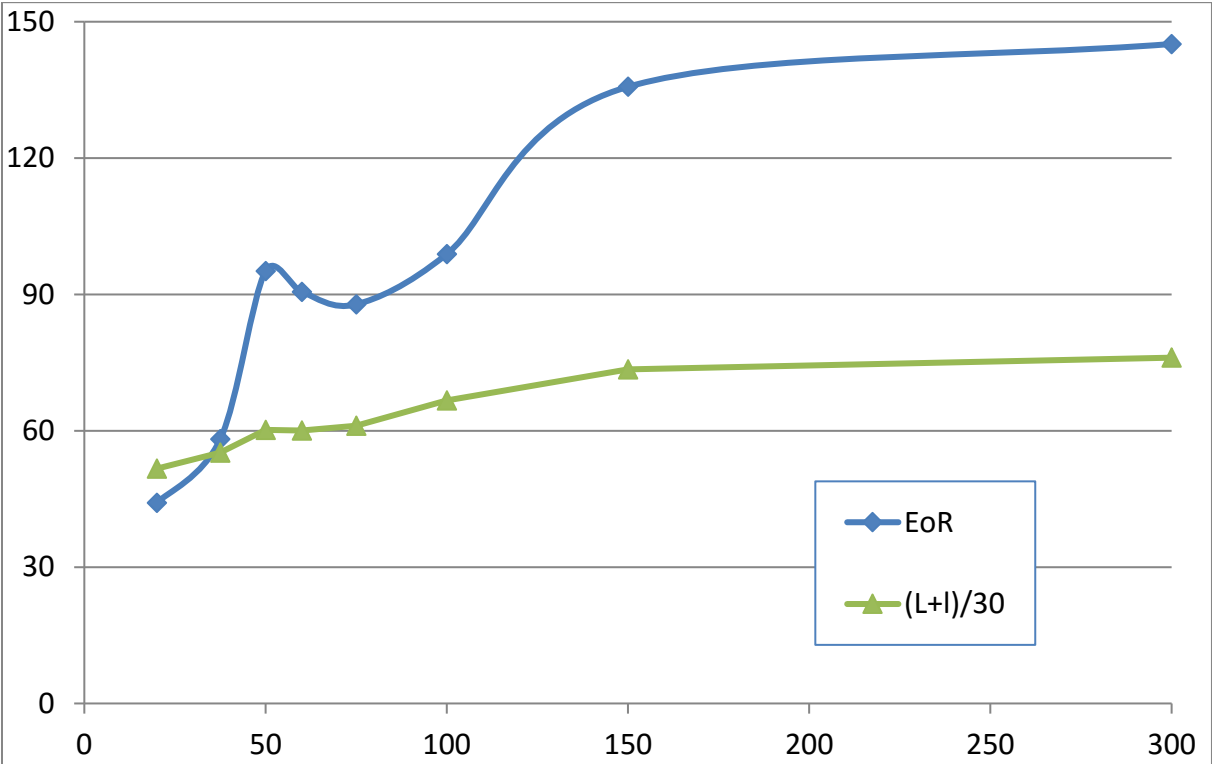


Figure 29: results of the mesh sensitivity analysis

As a result of this analysis, it is decided not to use shell finite element with a dimension higher than 750 mm. The aspect ratio  $r$  of the shell elements must not be too high, certainly not bigger than 2.

### 2.2.3 7,5 m x 15 m

The first slab panel presented here is a 7,5 m x 15 m slab panel with 2 unprotected IPE 600 in S235 parallel to the long edges, see Figure 30.

The chosen configuration fits nominally with the one described in Fig. 7.42, 6<sup>th</sup> solution, and Table 7.5 of the ECCS publication N°132.

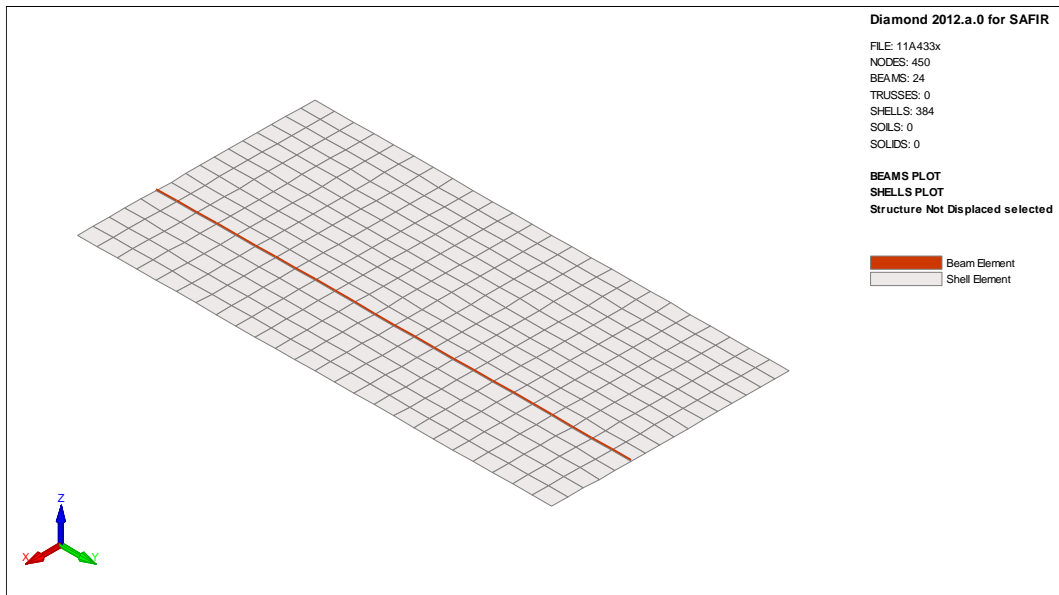
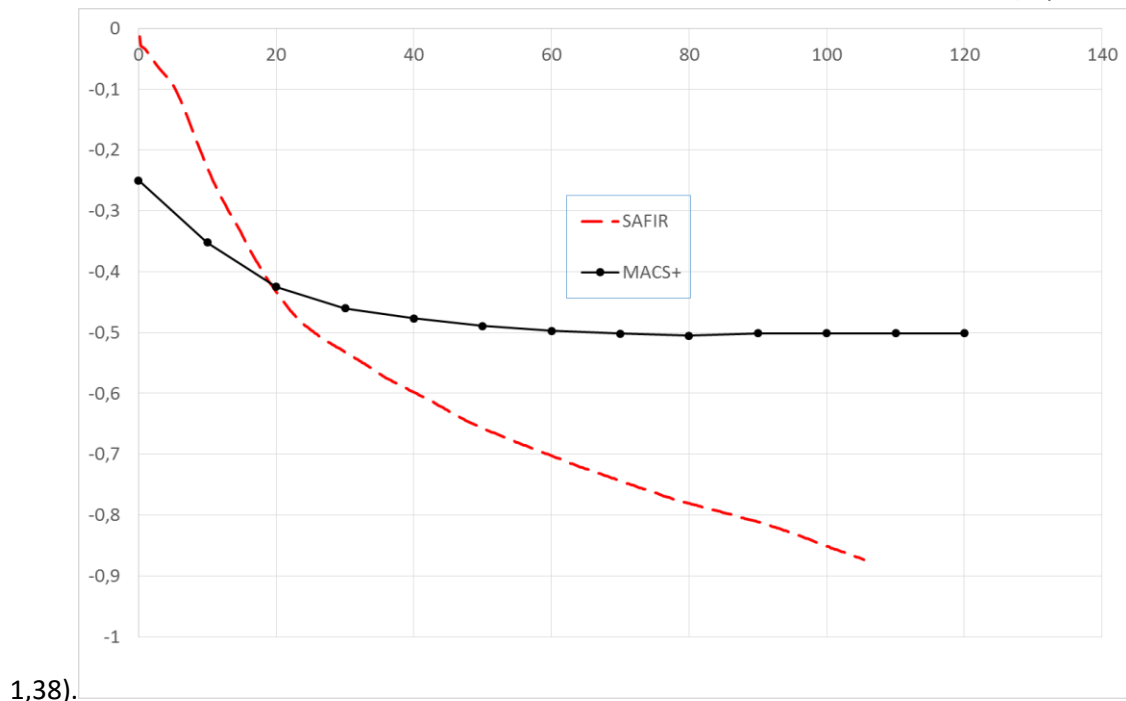


Figure 30: 7,5 x 15 m<sup>2</sup> (1/4 modelled)

1/4 of the slab panel was modelled owing to symmetry. The beam was modelled by 24 beam finite elements of 312,5 mm and 384 shell finite elements of 227 mm x 312,5 mm (aspect ratio :  $r =$



1,38).

Figure 31, for example, shows the evolution of the vertical displacement in the center of the slab calculated by SAFIR for a reinforcement of 473 mm<sup>2</sup>/m in each direction as recommended by Table 7.4 of the ECCS publication. The displacement calculated by MACS+ is also given in this Figure. It can be observed that, except during the first 15 minutes of the fire, the displacement calculated by MACS+ is lower than the one calculated by SAFIR. It has to be kept in mind that, in MACS+, the displacement is only an intermediate parameter used to calculate the enhancement factor; the bigger the displacement, the higher the enhancement factor and, hence, the higher the load bearing capacity at any given time.

SAFIR runs until 105 minutes, time when the strain in the unprotected steel beam reaches 15%; compared to a result of 110 minutes given by MACS+. The fact that the fire resistance time calculated by MACS+ is in the same order of magnitude as the one calculated by SAFIR is amazing considering that the displacement is underestimated by a factor of approximately 1,75 in MACS+. It seems as if some aspects of the mechanical part of the model in the simple method compensate in a way or another the underestimation of the vertical displacement.

It has yet to be discussed whether the displacement of 87 cm calculated by SAFIR after 105 minutes is acceptable, see Figure 33. The deflection is usually compared to the sum of the length of the short and of the long edge of the slab panel,  $l+L$ , considering that both primary and secondary beams that form the edges of the slab panel will deflect. Here the ratio after 105 minutes is  $(l+L)/26$ . Yet, if the edges of the slab panel are fixed vertically, which is the hypothesis of the simple method, the deflection that will be experienced in the building by the occupants will be related to the short edge as seen on Figure 32 and the ratio is then  $l/9$  ! At this moment, the horizontal displacement on the support, at mid distance of the long edge, is 118 mm, which means that the slab would most likely have lost vertical support.

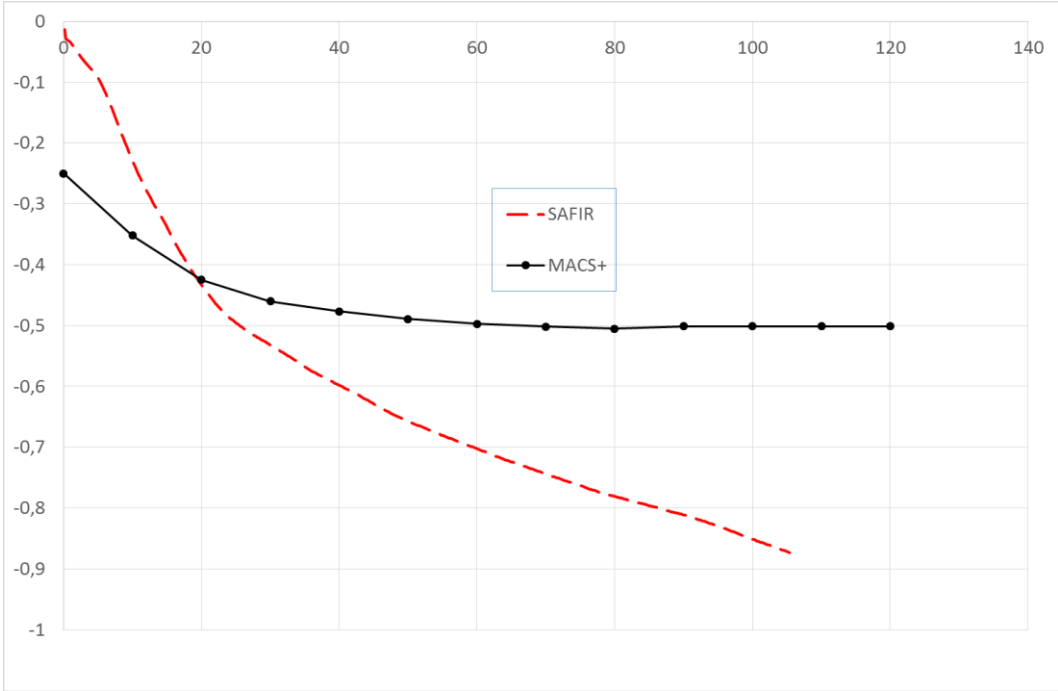


Figure 31: vertical displacement in the center of the 7,5 m x 15 m slab

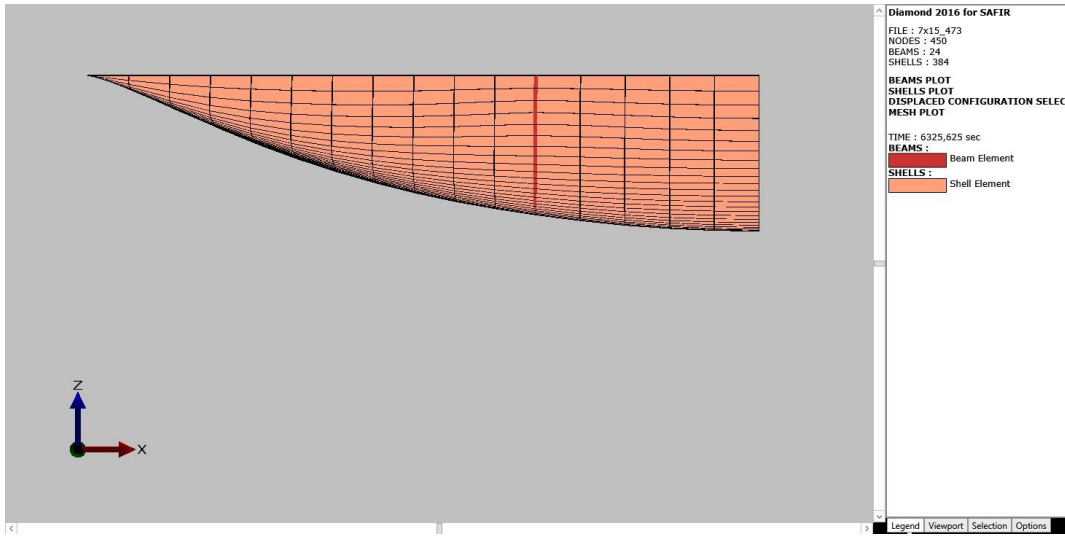


Figure 32: deformed shape after 105 minutes (side view)

Figure 33 shows the deformed structure after 105 minutes in an isometric view.

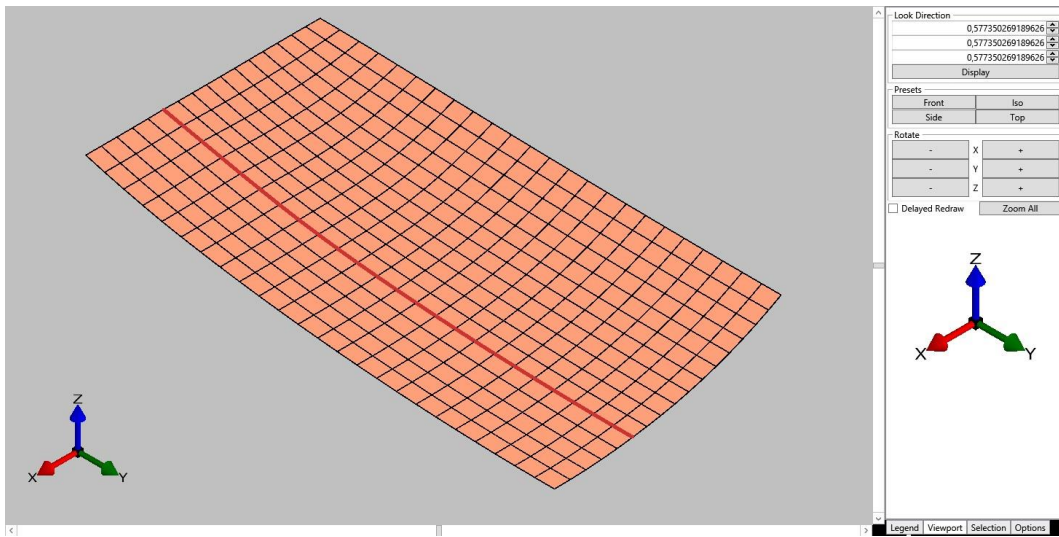


Figure 33: deformed shape after 105 minutes (isometry)

It is not uncommon to limit the deflection to  $(l/L)/30$ , equal here to 750 mm. In European testing standards, this deflection is calculated with respect to the position of the structure loaded before the fire (32 mm in Figure 31). In this report, we evaluated the deflection criteria with respect to the initial configuration, i.e. before loading. This is because the deflection calculated by SAFIR is obtained from a model in which the corrugated steel profiles are not present. Whereas this is in line with the hypotheses of the simple method and quite acceptable for the fire situation, this leads to an overestimation of the deflection at room temperature. It was decided here that this value of the deflection after loading can be neglected because, even if it is unknown, we know that it is smaller than the one calculated by SAFIR and hence quite negligible compared to  $(l+L)/30$ : here we know that the neglected deflection is less than  $32/750 = 4\%$ . The limit of 750 mm (corresponding to a ratio of  $l/10$ ) is observed after 72 minutes in SAFIR. The horizontal displacement on the support at that time is 85 mm.

In all results obtained by SAFIR, we will mention in this report the time when the  $(l+L)/30$  criteria has been met as well as the time at the end of the calculation with, if it can be determined, the reason that lead to an impossibility for SAFIR to calculate further.

Table 3 gives the results for different values of the rebar quantity, from 142 to 503  $\text{mm}^2/\text{m}$ .

In France, it is requested that the stress-related strain in the rebars does not exceed 5%. This value has been obtained in these simulations only for the two lowest reinforcement quantities, 142 and 200  $\text{mm}^2/\text{m}$ . In both cases, the end of run occurred within less than one minute after reaching 5% in the reinforcement. This means that this criteria, if it is applied, does not change the results of the simulations significantly.

It has been verified, for a reinforcement of 400  $\text{mm}^2/\text{m}$ , that the final resistance time is not significantly modified if steel in the beams is allowed to have an infinite plastic behavior (no descending branch). Compared to the steel of the EN 1993-1-2 where the plastic plateau is limited to 15%, the fire resistance time is only modified by 7 seconds. The displacement at the last converged step is somehow increased, from 1,012 meter to 1,074 meter. This exercise has been done to verify that the failure

times are not excessively influenced by the “numerical” problems that arise in the steel beam whereas, in reality, the slab could continue carrying the load for a longer time if the beam would just not be present. Clearly, this is not the case.

Table 3: results for the 7,5 m x 15 m slab panel

As mm <sup>2</sup> /m	MACS+	SAFIR EoR		SAFIR (L+I)/30
	min.	Min.	Reason	
142	22	21	No convergence	23
200	24	32	SdB in shell	31
250	25	39	No convergence	38
300	28	52	SdB in beams	48
350	34			55
375	40			58
400	60	91	SdB in beams	62
433	90	105	SdB in beams	66
473	111	105	SdB in beams	72
503	119	115	SdB in beams	76

Note: SdB means “Steel in Descending Branch” ( $\epsilon > 15\%$ ), EoR means “End of Run”, which is the time of last converged solution obtained by SAFIR.

Figure 34 shows the results in a graphic form. It can be observed that MACS+ yields safe results compared to the values provided by the numerical calculation if the end of run is considered. If a displacement limit is considered in the numerical calculations, MACS+ is still on the safe side for low reinforcement quantities (corresponding to R30 and R60) whereas it is not on the safe side for higher reinforcement quantities (corresponding to R90 and R120).

It has to be noted that, in order to consider the same hypotheses as MACS+, the numerical simulations have been performed with vertically fixed edge perimeters. If the deformation of the perimeter beams would be considered in the numerical simulations:

- 1) the numerical model would predict higher displacements than the displacements presented here;
- 2) there would be additional stresses in the concrete due to composite action with the perimeter beams.

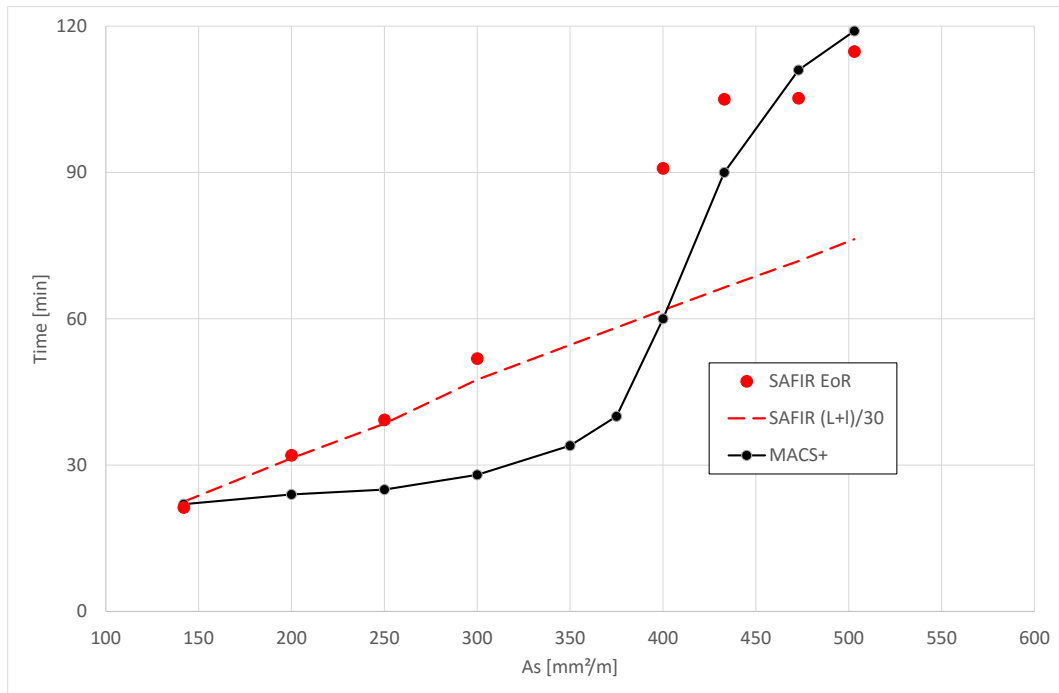


Figure 34: results for the 7,5 x 15 slab panel

### 2.2.4 9 m x 9 m

A 9 m x 9 m slab panel was then modelled, with 2 IPE 360 unprotected beams. The characteristic value of the life load considered here is 2,5 kN/m<sup>2</sup>. All other conditions are similar to the slab modelled in previous section. This corresponds to case N° 3 of Figure 7.42 in the ECCS document. The results are presented in Figure 36. ¼ of the slab was modelled owing to symmetry reasons. ¼ of a beam was modelled with 16 beam elements of 188 mm and 384 shell elements of 281 mm x 188 mm (aspect ratio  $r = 1,49$ ) see Figure 35.

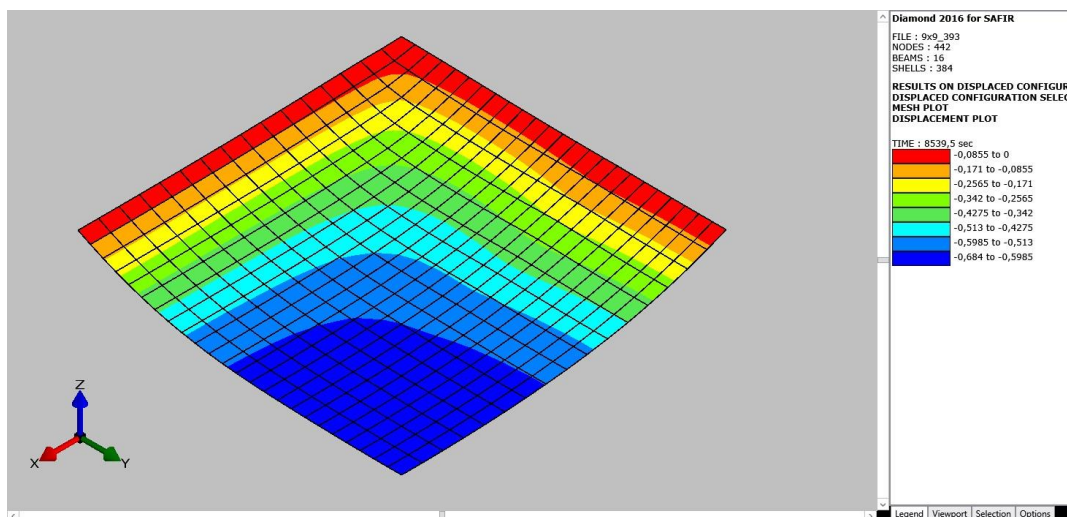


Figure 35: 9 m x 9 m model deformed

The results are presented on Figure 36 and in Table 4.

- The curve labelled “MACS+” represents the results of the Bailey-Moore method applied in the MACS+ software.
- The curve labelled “SAFIR (EoR)” presents the values obtained at the *End of Run* of the numerical calculation (last converged point).
- The curve labelled “SAFIR (L+I)/30” represents the time when the displacement criteria (L+I)/30 was met. The points of this curve located above the “EoR” curve have been obtained by linear extrapolation of the displacement curve beyond the last converged time.

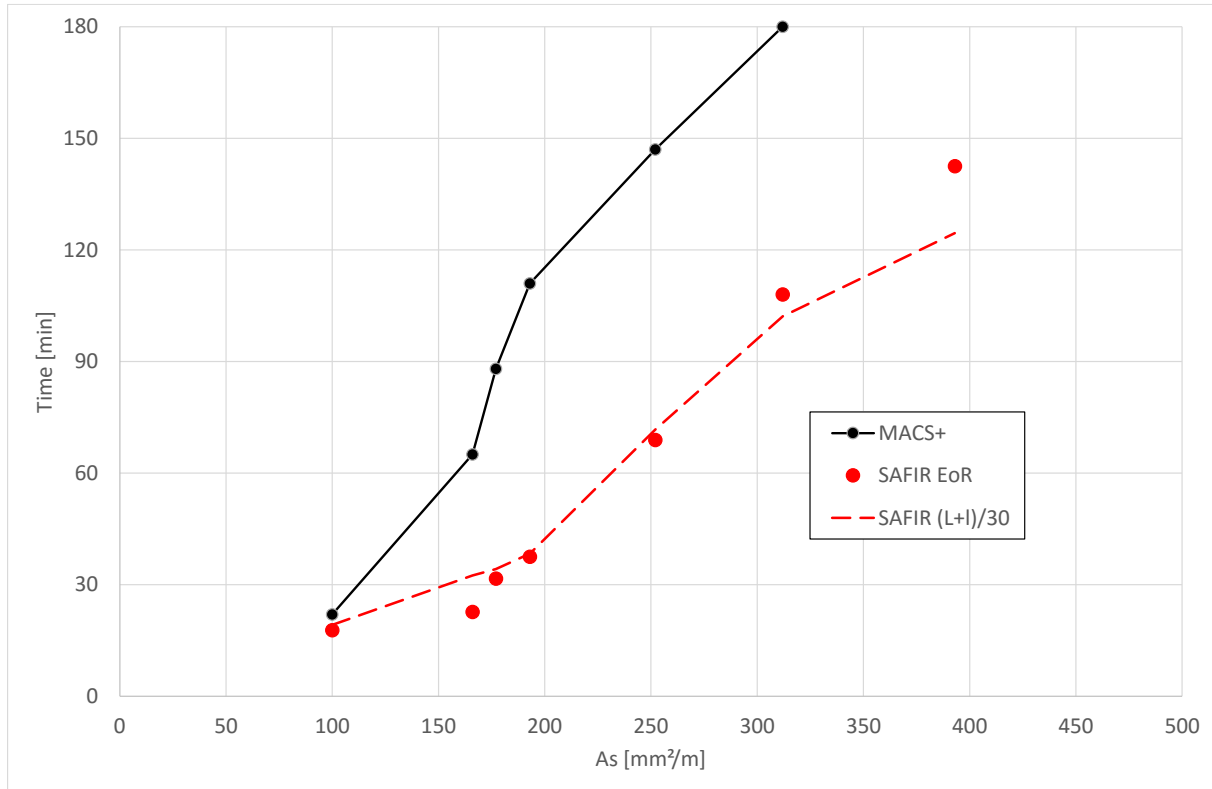


Figure 36: results for the 9 m x 9 m slab panel

Table 4: results for the 9 x 9 slab panel

As mm²/m	MACS+ min.	SAFIR EoR		SAFIR (L+I)/30 min.
		min.	Reason	
100	22	18	Strains in bars	19
166	65	23	SdB in the corner	33
177	88	32	SdB in the corner	34
193	111	38	SdB in the corner	38
252	147	69	SdB in the corner	72
312	180	108	SdB in beams	102
393		143	SdB in the corner	125

For this configuration, the end of convergence obtained by SAFIR was systematically obtained when the maximum deflection in the slab was close to (L+I)/30. In one single case (As = 100 mm²/m), a converged time step was obtained with the strain in a bar larger than 5%. The last converged step

followed only 12 seconds later. This means that failure was imminent in the numerical modelling when a value of 5% was reached for the elongation in the bars. This limitation does not change significantly the fire resistance time when it is applied.

The times calculated numerically, either for the deformation criteria or for the end of convergence, are smaller than the fire resistance times yielded by MACS+.

The difference is very small for  $A_s \approx 100 \text{ mm}^2/\text{m}$ , but the fire resistance time is not significant for this steel quantity because it is shorter than 30 minutes.

The difference is huge for higher steel quantities. For example,  $110 \text{ mm}^2/\text{m}$  are sufficient to yield R30 according to MASC+ whereas  $177 \text{ mm}^2/\text{m}$  are required according to SAFIR (+ 61%). If  $200 \text{ mm}^2/\text{m}$  are used, MASC+ gives a fire resistance time of nearly 120 minutes whereas SAFIR gives only 45 minutes. With  $300 \text{ mm}^2/\text{m}$ , MASC+ gives nearly 180 min when SAFIR gives only some 100 minutes.

The evolution of the displacement in the center of the slab as calculated by SAFIR and estimated by MACS+ is shown on Figure 37 for  $A_s = 193 \text{ mm}^2/\text{m}$ .

It has been mentioned that, for the rectangular slab of Section 2.2.3, the displacement was underestimated by MACS+ but the ultimate load bearing capacity was on the safe side compared to numerical modelling. For the square slab of this section, the displacement at failure is rather well estimated by MACS+ but the ultimate load bearing capacity is now very much on the unsafe side. This seems to confirm that the mechanical model of MACS+ based on the displacement could be unsafe and, when the displacement is underestimated, both errors tend to compensate each other.

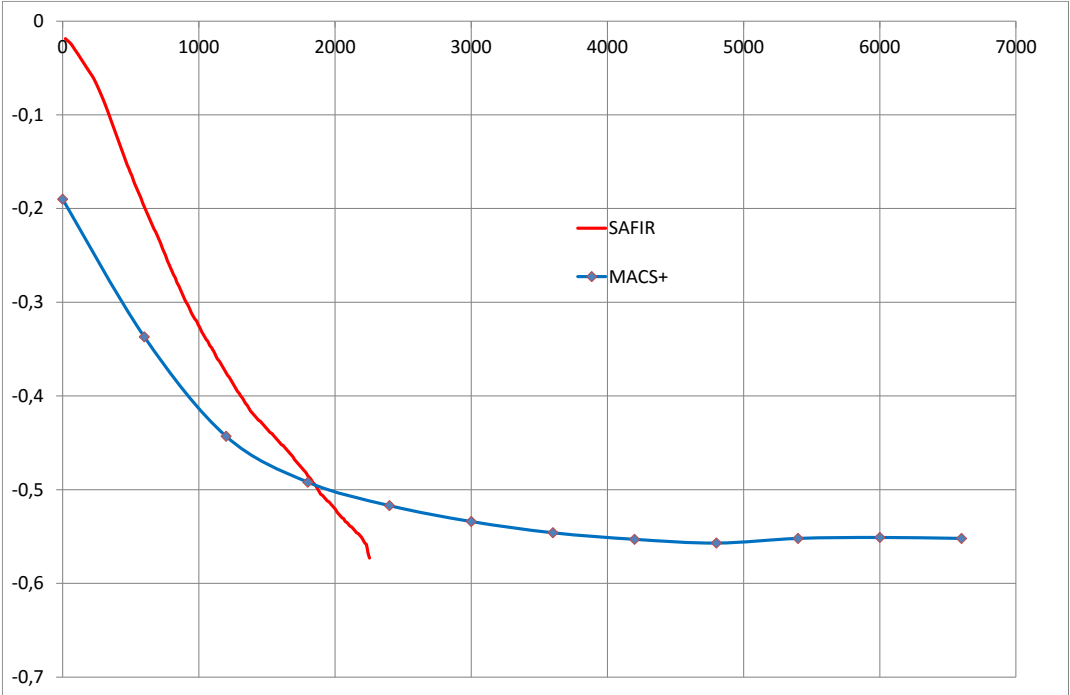


Figure 37: vertical displacement in the center of the 9 x 9 m² slab

## 2.2.5 6 m x 6 m

A slab panel of 6 m x 6 m with 1 unprotected IPE 270 in S235 has been analyzed. This configuration fits nominally with the one described in Fig. 7.42, 1<sup>st</sup> solution, and Table 7.5 of the ECCS publication N°132. ½ of the slab panel was modelled owing to symmetry. ½ of the beam was modelled by 10 beam finite elements of 300 mm and 1/2 slab by 200 shell finite elements of 307 mm x 302 mm (aspect ratio:  $r = 1,02$ ). Figure 38 shows the model deformed at the end of the run with a mesh of 125 mm<sup>2</sup>/m in each direction. The deflection at the center of the slab is equal to 479 mm. This deflection corresponds to  $l/13$ .

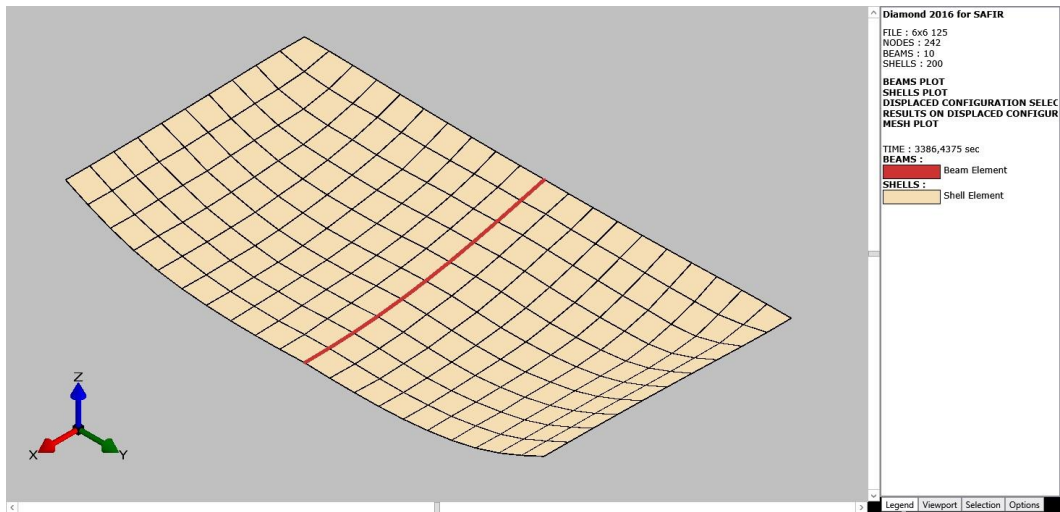


Figure 38: 6 m x 6 m model deformed

The results are given in Figure 39 and in the Table thereafter. The value of 5% for the mechanical strain in the reinforcing bars was not obtained in any of the simulations. The deflection  $(L+l)/30$  corresponds to a deflection of 400 mm. This deflection corresponds to  $l/15$ .

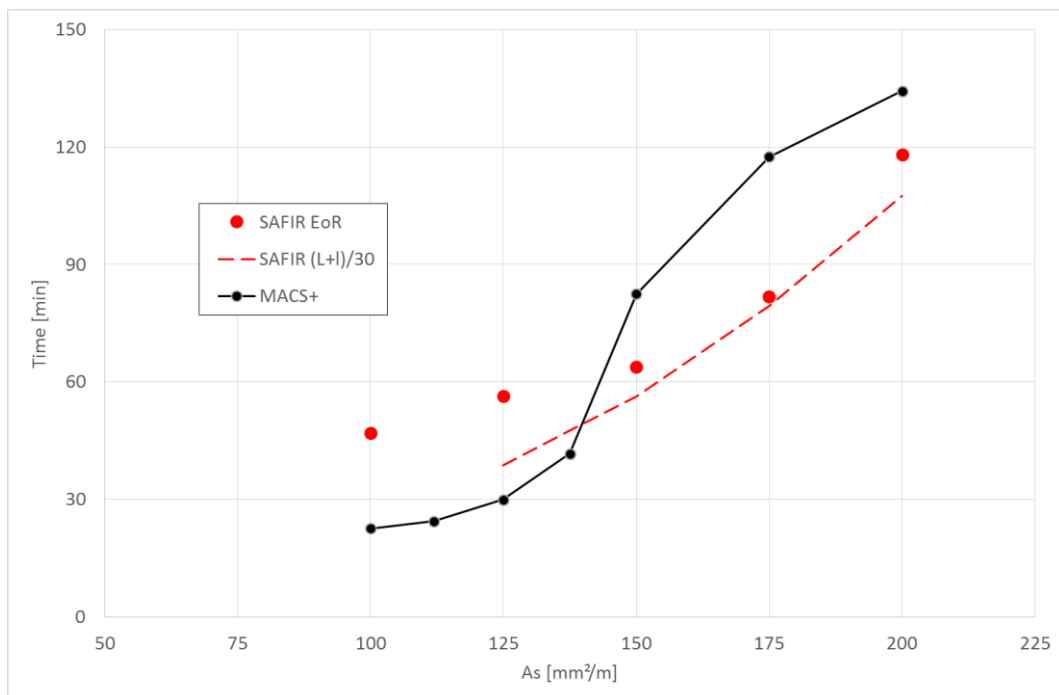


Figure 39: results for the 6 x 6 slab panel

As	MACS+	SAFIR EoR		SAFIR (L+l)/30
mm <sup>2</sup> /m	min.	min.	Reason	min.
100	23	47	SdB in the corner shell	
112	25			
125	30	56	SdB in beams	39
138	42			
150	83	64	Error in concrete	56
175	118	82	No convergence	79
200	134	118	SdB in the corner shell	108

### 2.2.6 6 m x 12 m

A slab panel of 6 m x 12 m with 1 unprotected IPE 600 in S235 parallel to the long edges has been analyzed. This configuration fits nominally with the one described in Fig. 7.42, 4<sup>th</sup> solution, and Table 7.5 of the ECCS publication N°132. The entire slab panel was modelled here. The beam was modelled by 24 beam finite elements of 500 mm and the slab by 384 shell finite elements of 500 mm x 375 mm (aspect ratio:  $r = 1,33$ ), see Figure 40.

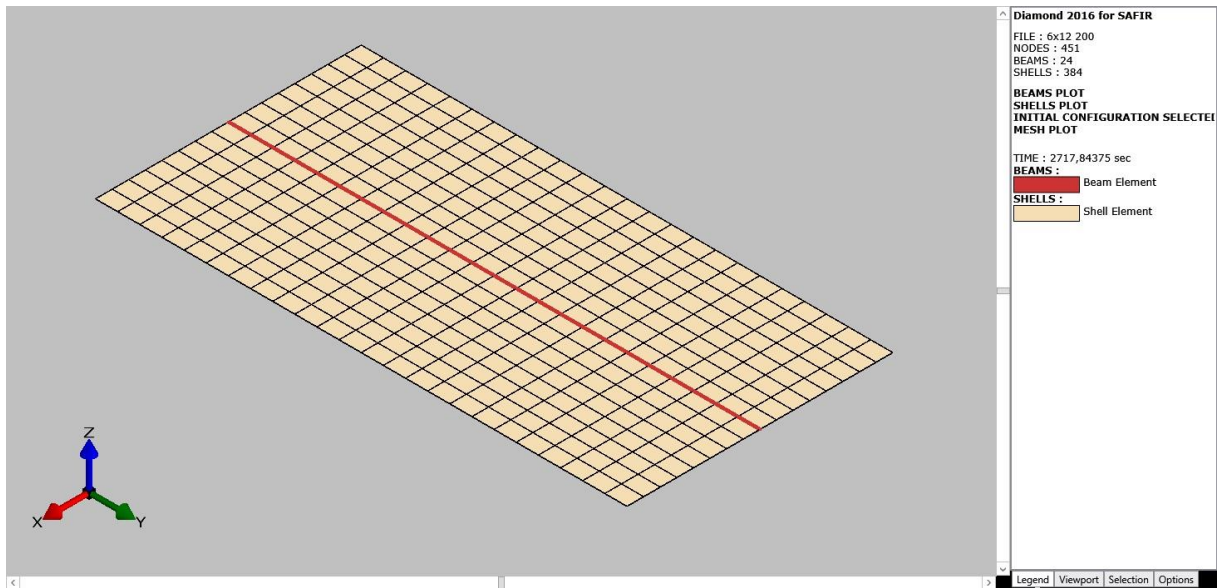


Figure 40: 6 m x 12 m model

The results are given in Figure 41 and in the Table thereafter. The value of 5% for the mechanical strain in the reinforcing bars was not obtained in any of the simulations. The deflection  $(L+l)/30$  corresponds to a deflection of 600 mm. This deflection corresponds to  $l/10$ .

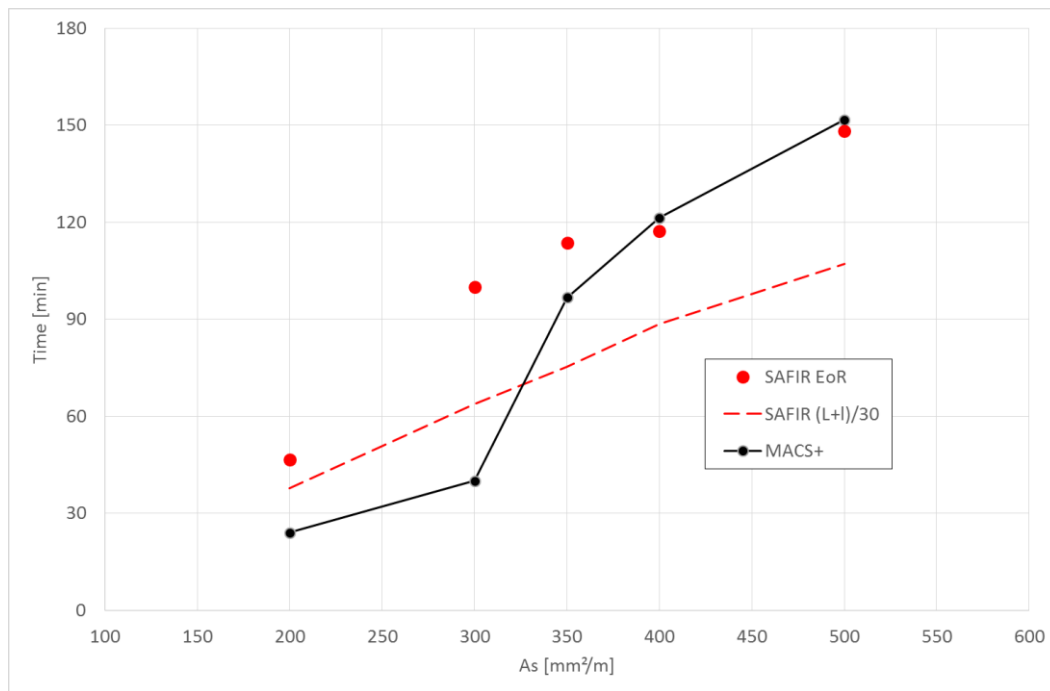


Figure 41: results for the 6 x 12 slab panel

As mm²/m	MACS+ min.	SAFIR EoR		SAFIR (L+I)/30 min.
		min.	Reason	
200	24	47	No convergence	38
300	40	100	SdB in beams	64
350	97	114	SdB in beams	75
400	121	117	SdB in beams	89
500	152	148	SdB in beams	107

### 2.2.7 9 m x 12 m

A slab panel of 9 m x 12 m with 2 unprotected IPE 600 in S235 parallel to the long edges has been analyzed. This configuration fits nominally with the one described in Fig. 7.42, 5<sup>th</sup> solution, and Table 7.5 of the ECCS publication N°132. ½ of the slab panel was modelled owing to symmetry. Each ½ beam was modelled by 12 beam finite elements of 500 mm and 1/2 slab by 216 shell finite elements of 500 mm x 500 mm (aspect ratio: 1,00). Figure 42 shows the model deformed when the deflection at the center of the slab is equal to  $(L+I)/30 = 700$  mm. This deflection corresponds to  $l/13$ .

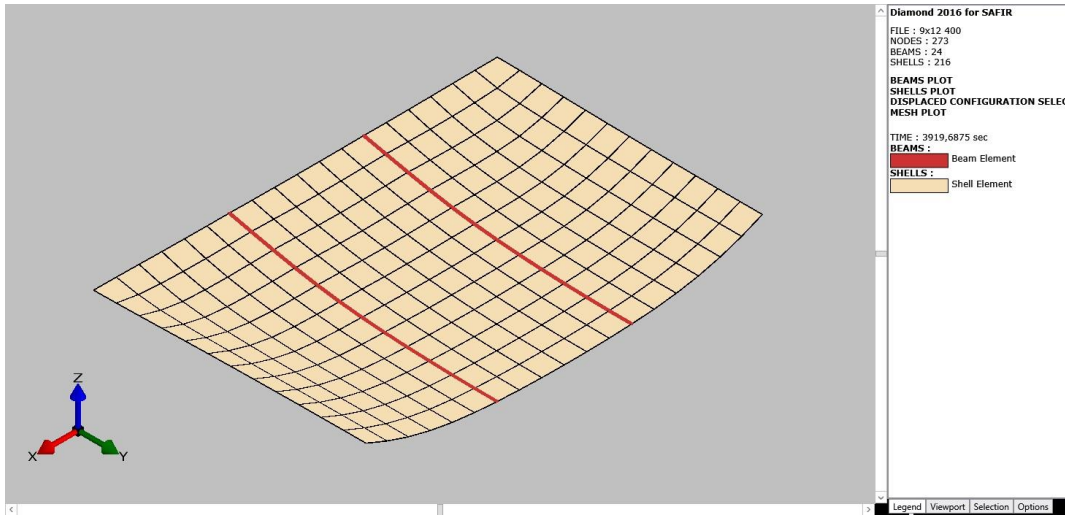


Figure 42: 9 m x 12 m model deformed

The results are given in Figure 43 and in the Table thereafter. The value of 5% for the mechanical strain in the reinforcing bars was not obtained in any of the simulations. For some simulations, the time corresponding to  $(L+l)/30$  is slightly longer than the time of the End of run. For these cases, the time corresponding to  $(L+l)/30$  has been extrapolated beyond the End of Run in the time-displacement curve.

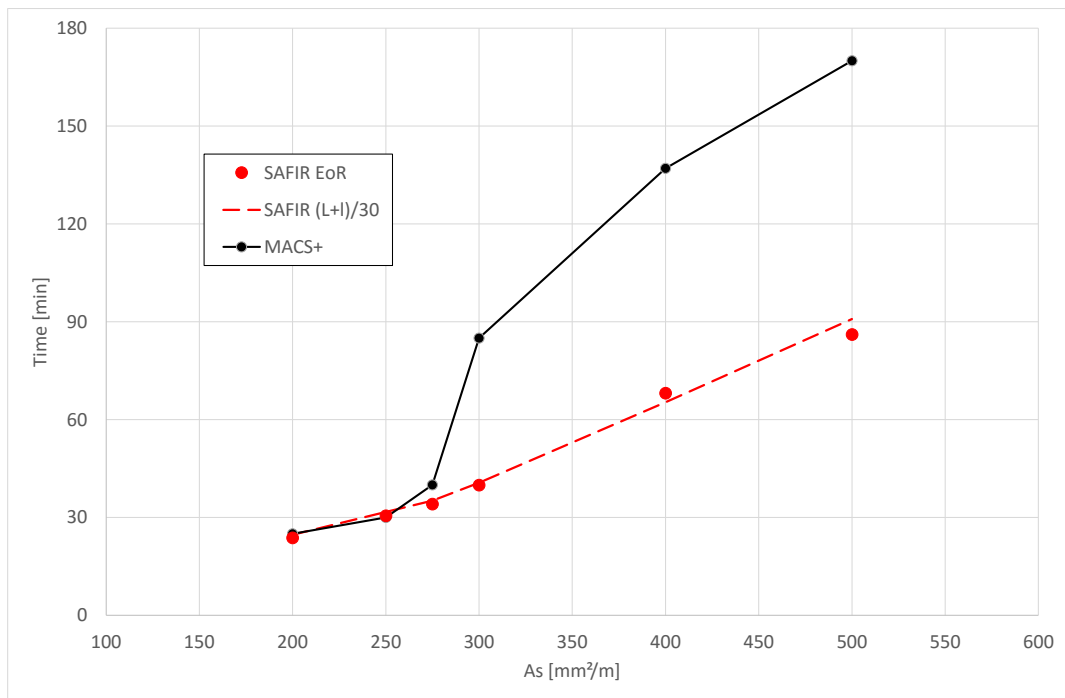


Figure 43: results for the 9 m x 12 m slab panel

Results for the 9 m x 12 m slab panel

As mm <sup>2</sup> /m	MACS+ min.	SAFIR EoR		SAFIR (L+l)/30
		min.	Reason	min.
200	25	24	No convergence	25
250	30	31	No convergence	32
275	40	34	No convergence	35
300	85	40	SdB in the corner	41
400	137	68	No convergence	65
500	170	86	SdB in beams	91

### 2.2.8 9 m x 15 m

A slab panel of 9 m x 15 m with 2 unprotected IPE 500 in S235 parallel to the long edges has been analyzed, see Figure 44. This configuration fits nominally with the one described in Fig. 7.42, 7<sup>th</sup> solution, and Table 7.5 of the ECCS publication N°132. The entire slab panel was modelled here. Each beam was modelled by 20 beam finite elements of 750 mm and the slab by 300 shell finite elements of 600 mm x 750 mm (aspect ratio :  $r = 1,25$ ).

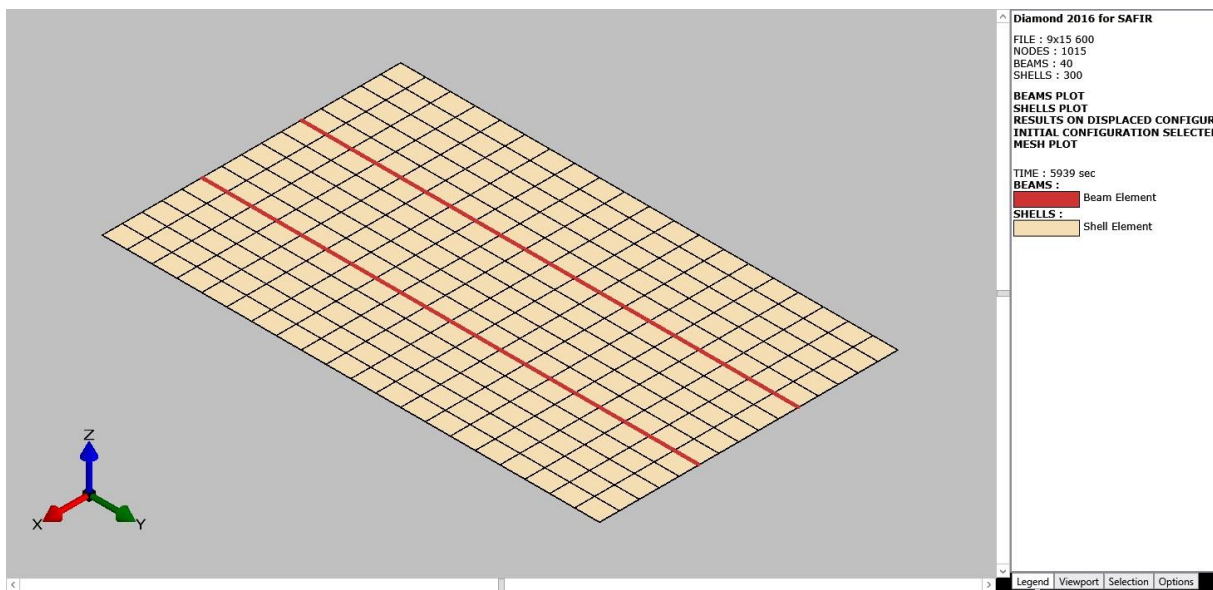


Figure 44: 9 m x 15 m model

The results are given in Figure 45 and in the Table thereafter. The value of 5% for the mechanical strain in the reinforcing bars was not obtained in any of the simulations. The deflection  $(L+l)/30$  corresponds to a deflection of 800 mm. This deflection corresponds to  $l/11$ .

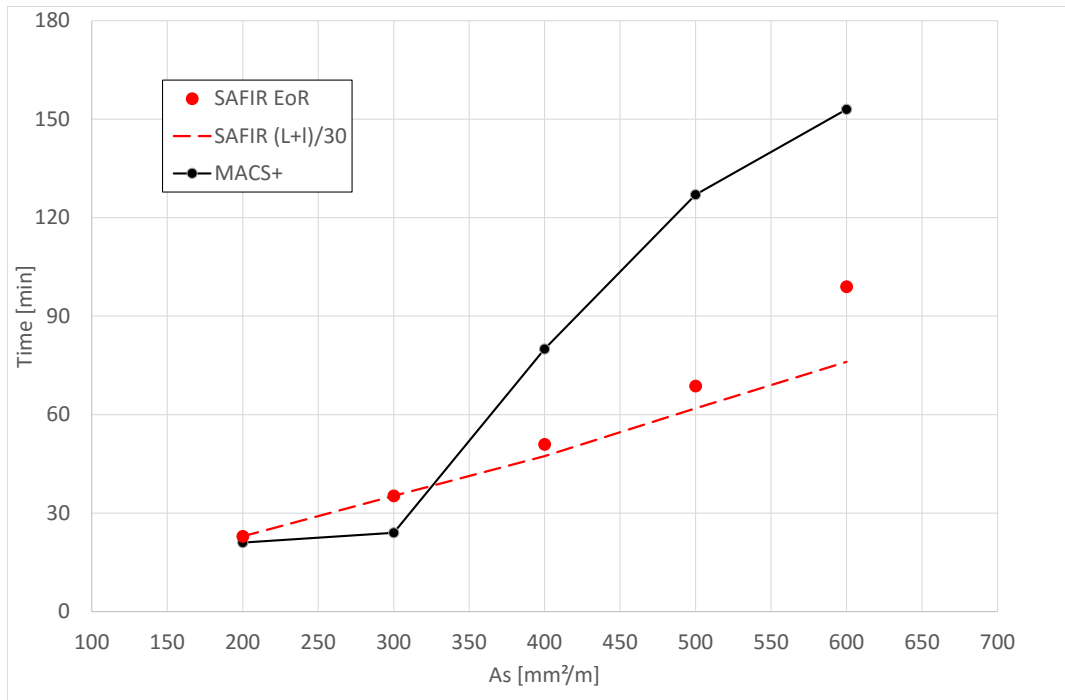


Figure 45: results for the 9 x 15 slab panel

Results for the 9 m x 15 m slab panel

As	MACS+	SAFIR EoR		SAFIR (L+I)/30
mm²/m	min.	min.	Reason	min.
200	21	23	No convergence	23
300	24	35	No convergence	35
400	80	51	No convergence	47
500	127	69	SdB in beams	62
600	153	99	SdB in beams	76

### 2.2.9 3 sides heating versus 4 sides heating

All simulations performed in the ECCS document as well as in this document are performed with a composite slab made of a COFRA\*60 steel sheet. Because this sheet covers less than 90% of the upper flange of the steel section, the steel section is heated on 4 sides.

Yet, if the steel sheet is a reentrant profile (e.g. *Hollerith* type), more than 90% of the upper flange is covered by the composite slab and the steel beams have to be modelled as exposed to three sides only. This will induce a thermal gradient in the steel beam that is likely to increase the vertical displacements in the slab panel. We investigated whether this could have a detrimental effect on the behavior of the slab panel.

The temperatures in the IPE360 beam have been calculated on the hypothesis that it is heated on 4 sides first, see Figure 46, then on 3 sides, see Figure 47.

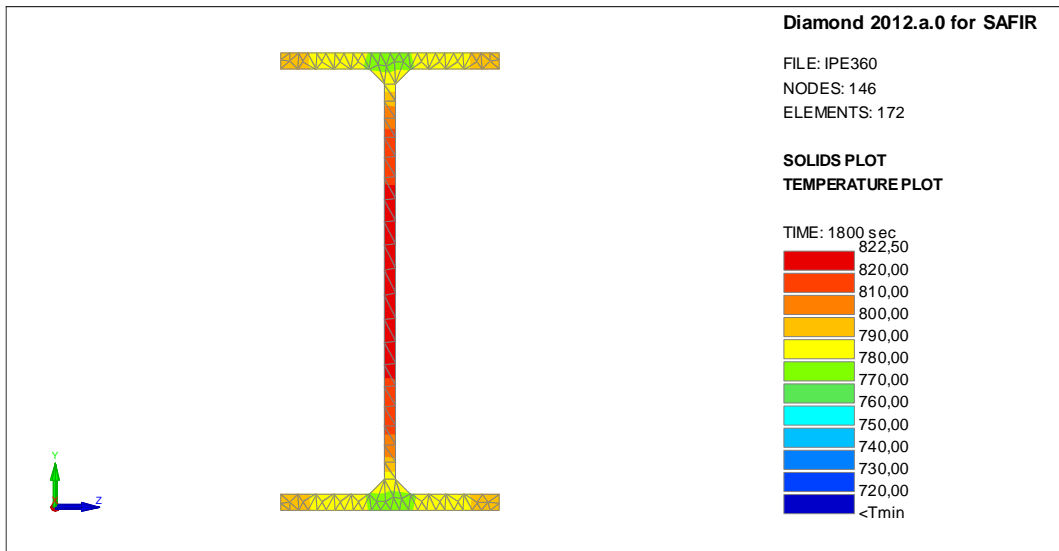


Figure 46: temperatures after 30 minutes (4 sides heated)

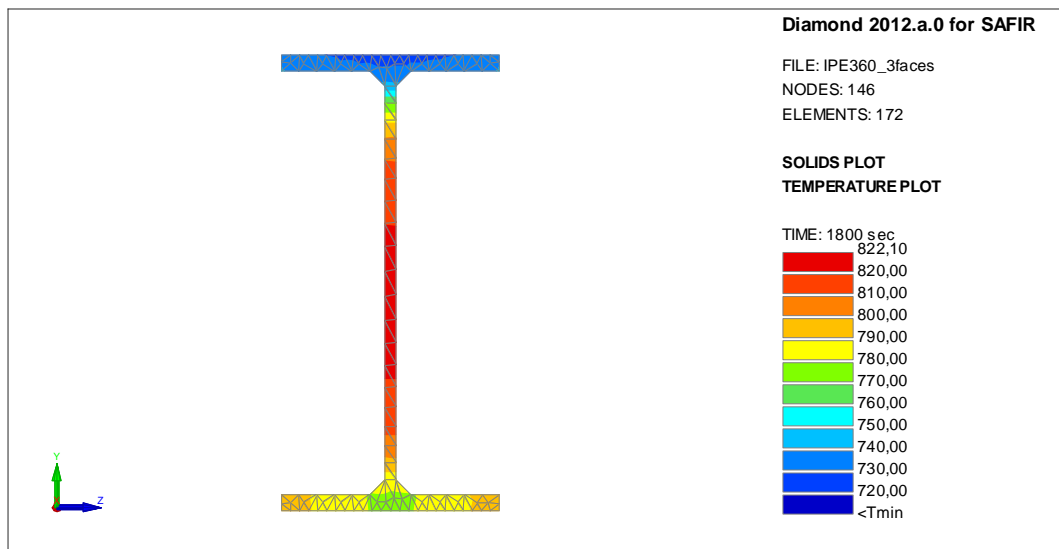


Figure 47: temperatures after 30 minutes (3 sides heated)

The 9 m x 9 m slab panel with reinforcement of 193 mm<sup>2</sup>/m has been calculated on the base of these two hypotheses. The evolution of the displacement in both hypotheses is presented in Figure 48.

The displacement is indeed slightly bigger when the beams are heated on 3 sides but not to an extent that would affect significantly the time when a displacement criterion would be met. The time of failure (last converged point) is higher with 4 sides exposure (1 min 30 sec), with the displacement being the same when the vertical asymptote begins.

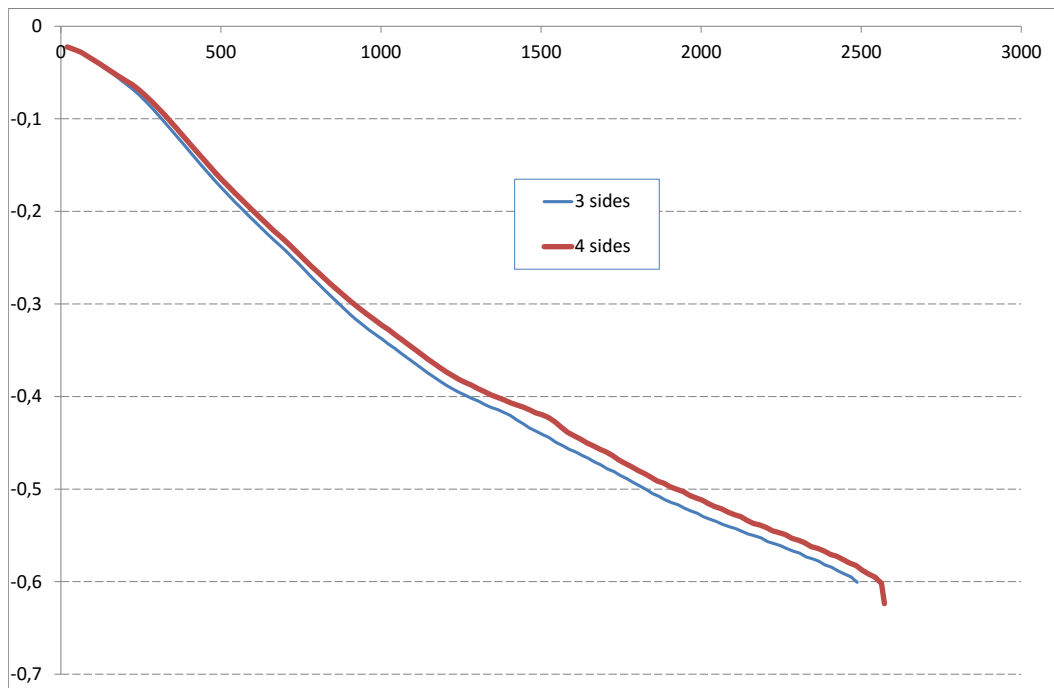


Figure 48: 3 sides/4 sides heating

### 2.2.10 Influence of lack of overlap

In order to investigate the possible effect of a lack of overlap between two reinforcing meshes, a model has been made of the 7,5 m x 15 m slab with  $433 \text{ mm}^2/\text{m}$  of steel where an initial crack of 2 meters length was introduced from the beginning in the model. This was achieved by releasing the restraint of several nodes located in one plane of symmetry; see the restraint in the Y direction on nodes 422 to 425 in Figure 49.

This simulates a total lack of overlap between adjacent reinforcing meshes on a line that is 2 meters long in the center of the slab panel, perpendicular to the unprotected steel beams. In a real situation, concrete would be present on this line and there would be no crack in the initial stage, but concrete would crack very soon during initial loading or, at least, as soon as any tensile force would develop.

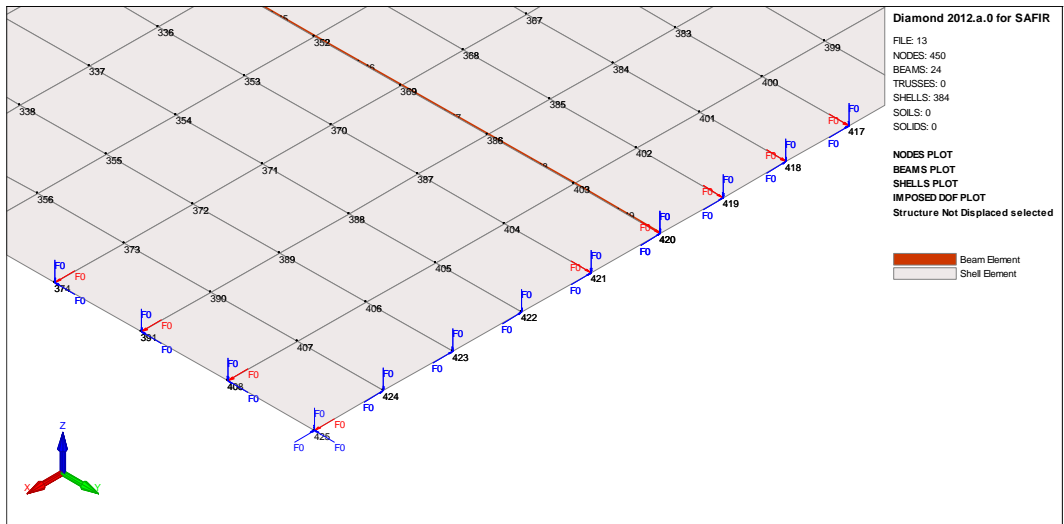


Figure 49: model with initial crack

Figure 50 shows the evolution of the vertical displacement with a good overlap and with a lack of overlap. There is no influence in the initial stage when bending perpendicular to the steel beams and thermal stresses dominate, but a difference appears when the tensile membrane action is being established. There is an influence of the time when the simulation stops (by steel in the descending branch in the beam for both cases) from 114 to 95 minutes as well as on the time when the  $(I+L)/30$  criteria is met, from 77 to 65 minutes. Yet, no catastrophic failure occurs at a very early stage. This result is in line with the observations in experimental tests FRACOF and the office demonstration test of Cardington.

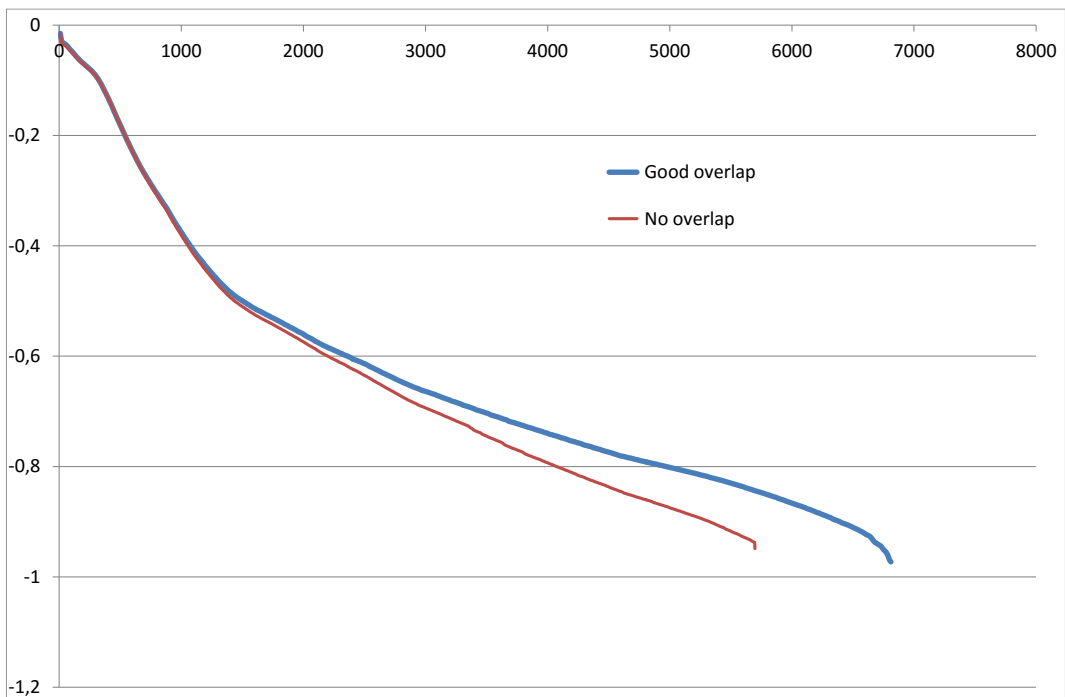


Figure 50: influence of overlap

Figure 51 shows the distribution of membrane forces around the crack at failure. The tensile forces perpendicular to the crack are indeed very small as expected<sup>9</sup>, but it is interesting to note the compression forces that appear parallel to the crack.

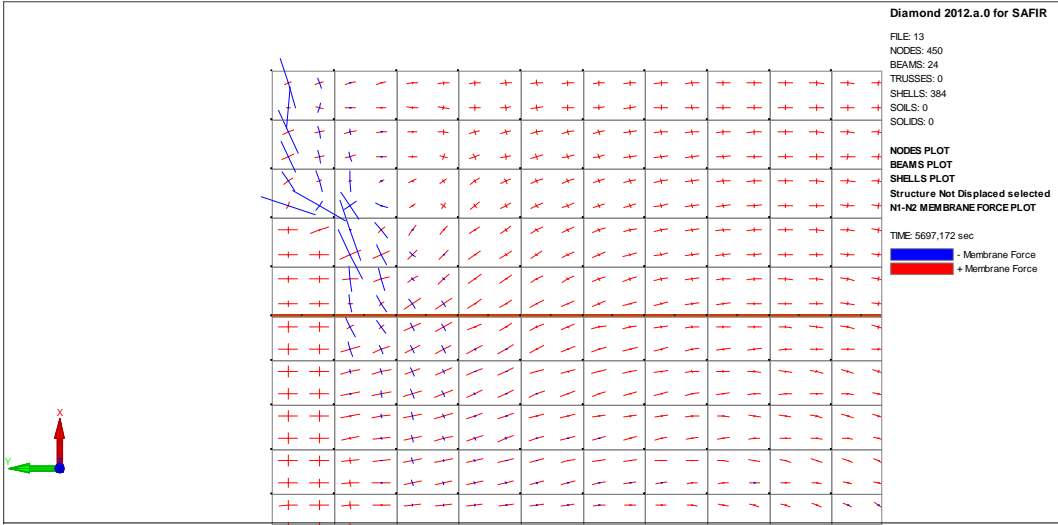


Figure 51: membrane forces around the crack

The considerations mentioned above in this section are related only to the load bearing capacity *R*. A crack caused by a lack of proper overlap would also influence the integrity criteria *E*. Figure 52 shows the evolution of the displacement in the direction perpendicular to the crack, for the nodes that define the crack. Because the crack is located on an axis of symmetry, the opening of the crack is twice the value presented here. It can be observed that the influence on the integrity might be significant at a quite early stage in the fire. An opening of 1 cm ( $2 \times 0,005$  m) is here observed after 20 minutes of fire.

<sup>9</sup> They would be null with a finer mesh.

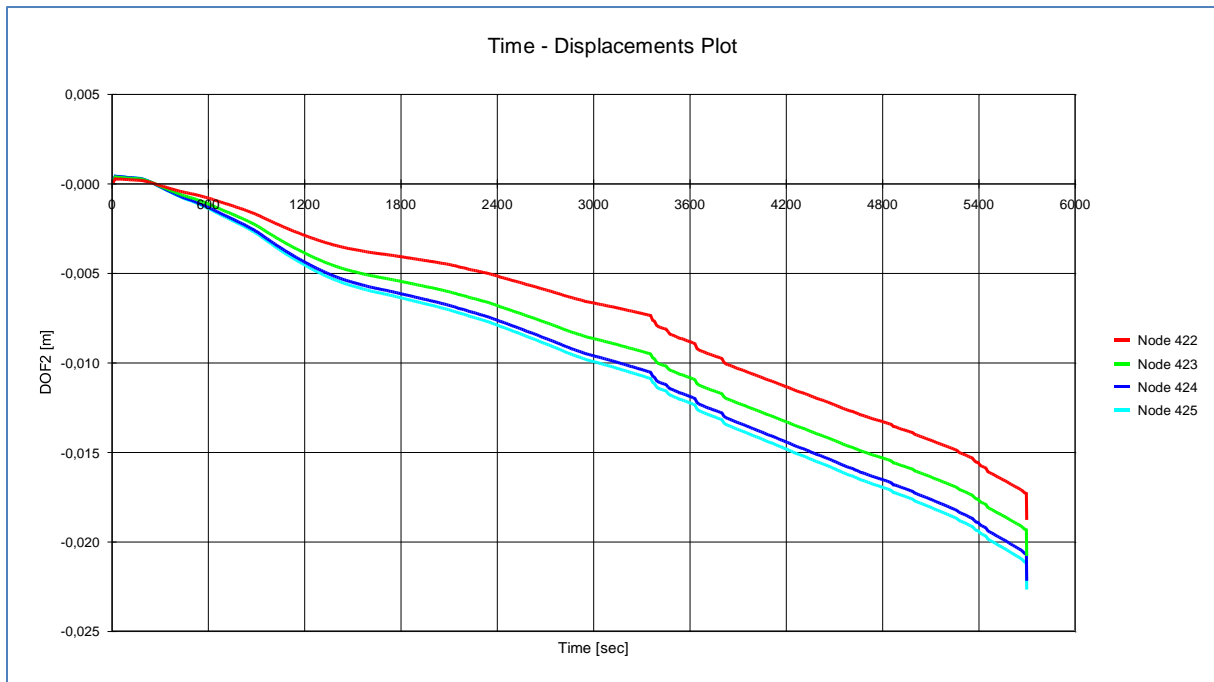


Figure 52: 1/2 of the opening of the crack

Other crack sizes, locations or directions would produce other effects. It is not within the scope of this report to present a comprehensive study about this phenomenon.

### 2.2.11 Effect of a localized fire

In order to investigate the response of a slab panel under localized fires, two slab panels were analyzed under a Hasemi localized fire, see Annex C of EN 1991-1-2, located 3 meters underneath the 9 m x 9 m slab with 252 mm<sup>2</sup>/m of steel. The diameter of the fire is 4 meters and the rate of heat release is 6.2 MW (both constant).

First, the slab has been analyzed with the fire located in the center of the slab. After 2 hours, the temperature has reached a steady state situation. The steel beam temperature varies from 260°C at the supports to 695°C at mid span. The temperature in the reinforcement of the slab varies from 82°C in the corner of the slab panel to 362°C in the center of the slab panel.

Second, the slab has been analyzed with the fire located in a corner of the slab (precisely at 1,5 meter from the corner in both directions). Because symmetry is not present in this case, the whole slab panel was modelled.

Figure 53 presents the evolution of the vertical displacement in the center of the slab panel for the ISO fire and for the local fire located in the center, and in the point with highest deflection for the local fire located in the corner. It shows that the local fires did not induce collapse of the slab panel, on the contrary to the ISO fire.

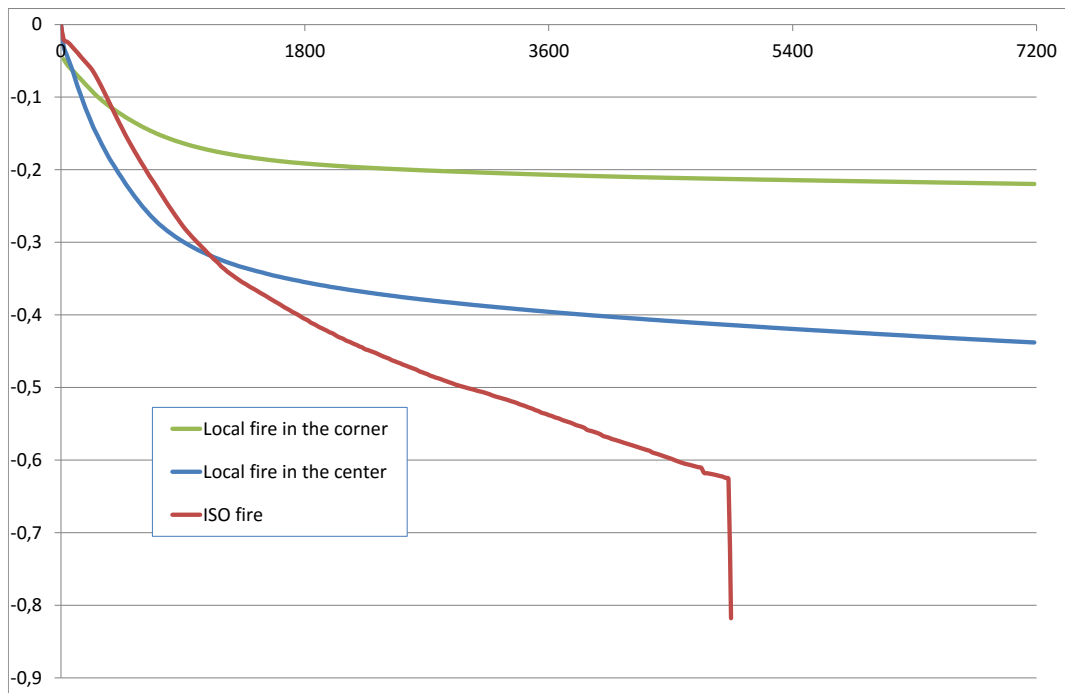


Figure 53: ISO versus localized fires

Figure 54 and Figure 55 show the deformed shape of the slab under localized fire after 2 hours whereas Figure 56 presents the deformed shape for the last converged point under ISO fire. The highly distorted elements in the corner suggest that failure of the slab has been really reached, see vertical asymptote on Figure 53.

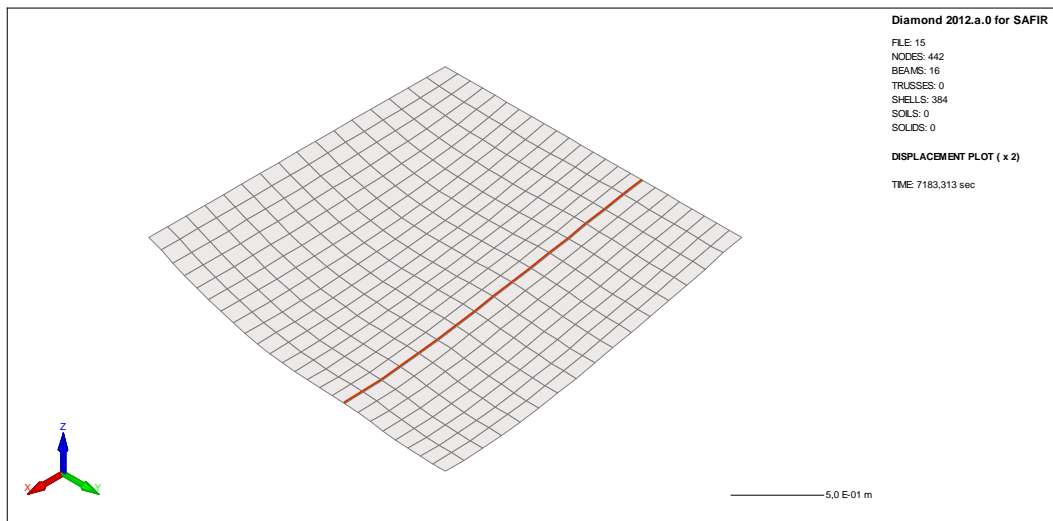


Figure 54: displacement under localized fire in the center (x2)

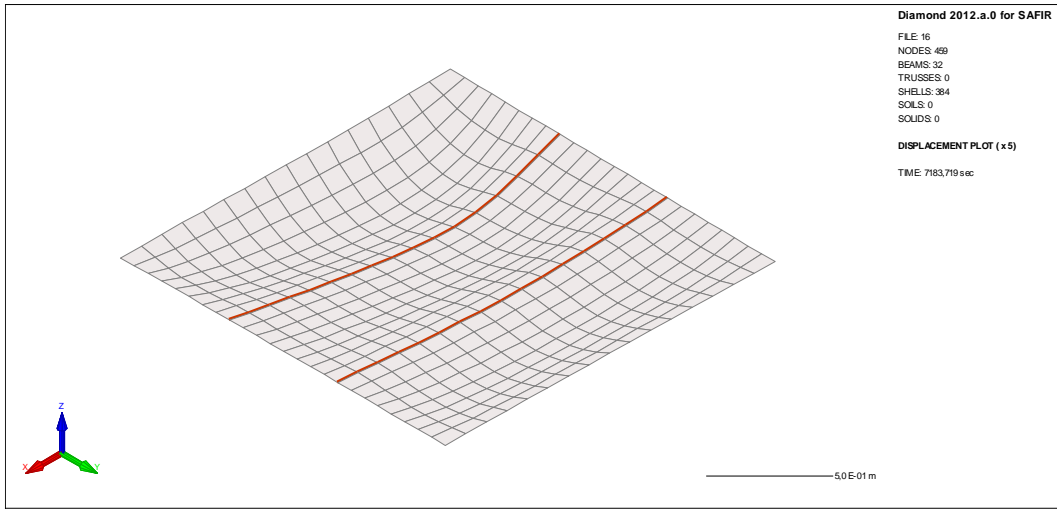


Figure 55: displacement under localized fire in the corner (x5)

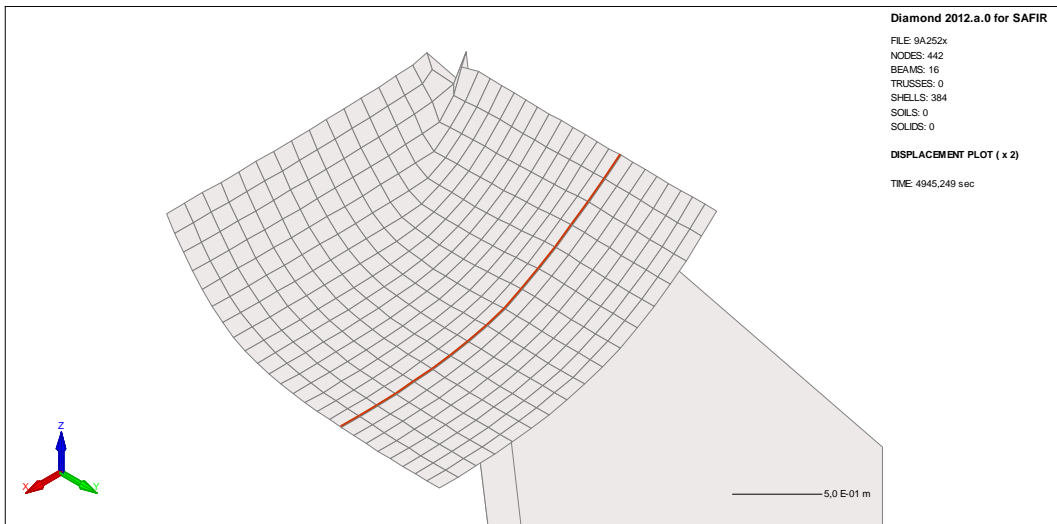


Figure 56; displacement under ISO fire (x2)

Figure 57 shows the membrane forces under localized fire in the center after 2 hours whereas Figure 58 shows the membrane forces under ISO fire at the last converged point. No significant membrane forces develop when the localized fire is in the corner.

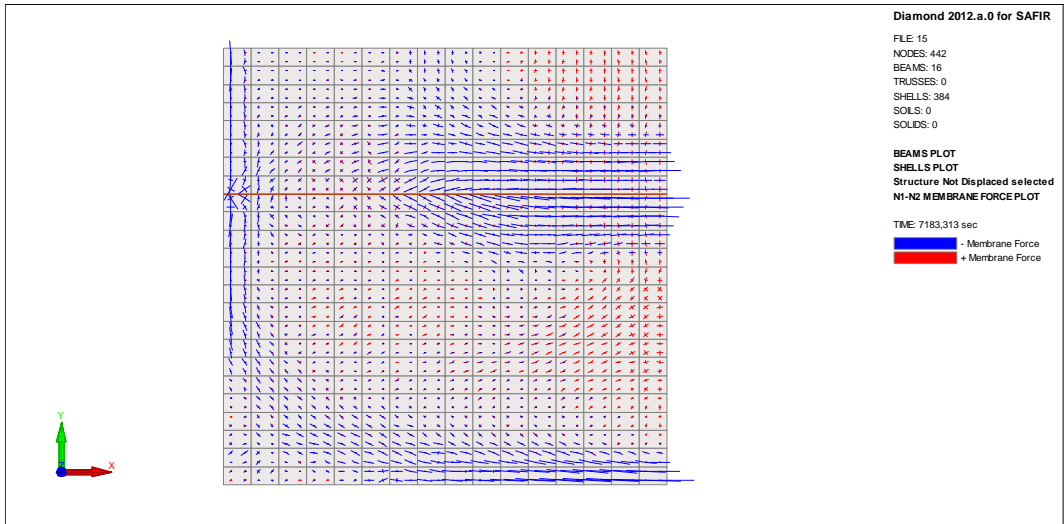


Figure 57: membrane forces under local fire

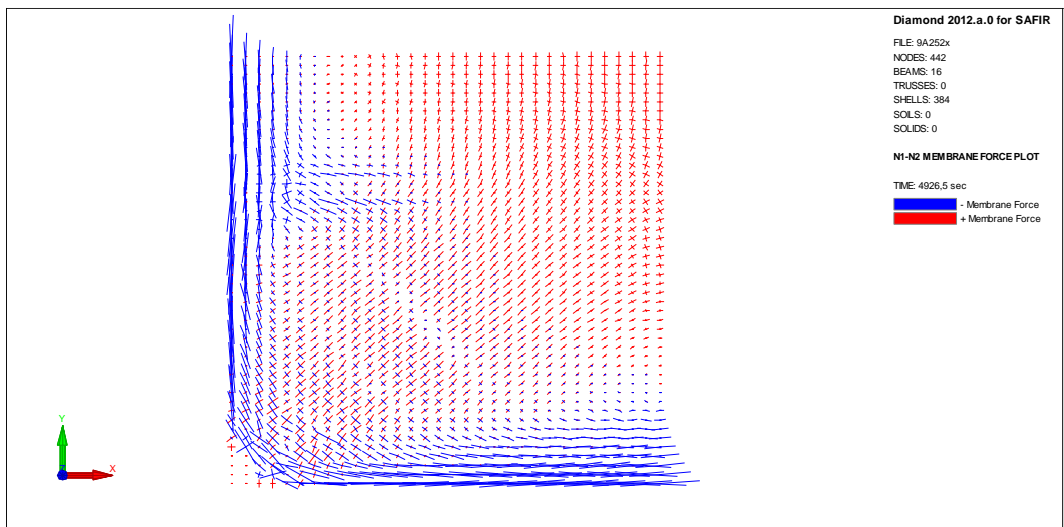


Figure 58: membrane forces under ISO fire

## 3 Conclusions

### 3.1 Tensile membrane action

Our simulations showed, as many other simulations performed by various authors before as well as several experimental tests, that tensile membrane action is a real load transfer mode that allows supporting loads applied on slab panels with much larger dimensions than bending transfer mode would.

The fact that the unprotected steel beams located in the central part of the slab panel are heated on 3 sides or heated on 4 sides does not appear to have a significant influence.

Two simulations performed tend to show that tensile membrane action can also develop if the slab panel is subjected to a localized fire.

The influence of a lack of reinforcing bar cover may affect the load bearing capacity, criteria R. This appeared if a deformation criterion is considered as well as for the ultimate fire resistance time (last converged point). The important crack that may develop in case of a lack of cover is likely to be detrimental for the integrity criterion E as well.

It would be wise to give some recommendations to be followed on site when tensile membrane action has been considered in the fire design: level of control of the workers, ductility of the reinforcing bars, verification of the cover of the prefabricated welded steel meshes... Maybe the positioning of these steel meshes should not be left to the appreciation of the workers on site but should be decided by the designer and clearly indicated on the drawings. Indeed, execution imperfections have been observed even in the supposedly well controlled environment of research programs such as *“reinforcement ... not been lapped correctly”* in the office demonstration test of Cardington, *“reinforcing mesh” not “properly overlapped”* in the FRACOF test, a *“defective fire protection”* on a perimeter beam in the COSSFIRE test. It is remarkable yet that, in none of these three tests, the constructional imperfections lead to a catastrophic failure of the structure.

### 3.2 The Bailey-Moore simple method

This method is based on a combination of hypotheses, some on the kinematic of the problem and some on the static of the problem. Therefore, it is not possible to know whether the obtained load capacity in the fire situation is systematically on the safe side or on the unsafe side, as is the case with the purely kinematic or purely static approaches of the plastic theory.

Furthermore, some of these hypotheses are either not justified or they contradict each other, see annex.

Also, the method has been tuned by the introduction of a fitting coefficient in order to improve correspondence between the results that it produces and the results of a certain series of experimental tests. It is not certain whether this fitting coefficient is appropriate for configurations different than those of the series that has been used for the calibration.

It can thus not be stated that this method is fool proof in terms of structural mechanics.

This method belongs clearly to the family of simple calculation methods, as opposed to the families of tabulated data or advanced calculation models in the sense of the Eurocodes. We base this appreciation on the fact that the method is based on a series of global equilibrium equations that can be solved “by hand”. Tabulated data, on the contrary, are tables or formula based on best fit with results produced by experimental tests or by more advanced methods, which is not the case for this method<sup>10</sup>. Advanced calculation models are based on principals of structural mechanics applied at the local level. This is not the case for this method<sup>11</sup>.

The results of this method applied with the MACS+ software described in Section 3.3 have been compared with the results of nonlinear numerical simulations performed with our software SAFIR®. This software belongs to the family of advanced calculation models and served here as a point of reference. Six slab configurations have been analyzed with the quantity of steel reinforcement being varied in each configuration. Our comparisons confirmed the finding already mentioned in Huang, Burgess, Plank & Bailey, 2004<sup>12</sup> that we quote here: “... *the simple design method may predict greater fire resistance ... than ... [numerical] modelling. This is particularly the case for highly reinforced square slabs... Cases with [less] reinforcement, as well as the less square slabs, show less enhancement and the disparity is less apparent.*”

In fact, this is exactly what was found here for the square slab panels of 9 m x 9 m (see Figure 36) and 6 m x 6 m (see Figure 39). Except for very low steel quantities, the simple method yields a fire resistance that varies from 2 to nearly 3 times the fire resistance given by numerical modelling.

For a slab with an aspect ratio  $r$  of 2, in this case 7,5 m x 15 m (see Figure 34) and 6 m x 12 m (see Figure 41), our simulations also confirm the findings of Huang et al., 2004. The simple method yields results that are on the safe side compared to numerical modelling, at least for the lower reinforcement leading to fire resistance times up to 60 minutes. For higher reinforcement ratio leading to longer fire resistances, the results of the simple method are between the numerical results if a displacement criteria of  $(l+L)/30$  is applied and the numerical results if only the last converged point is considered.

Slab panels with intermediate aspect ratio, here 9 m x 12 m ( $r = 1,33$ , see Figure 43) and 9 m x 15 m ( $r = 1,67$ , see Figure 45) show a behavior that is intermediate between the one of square panels and the one of panels with an aspect ratio of 2.

We think personally that this method is a valuable tool for yielding a preliminary design of a slab panel working in tensile membrane action under fire, but the design should then be verified and finalized by a test or by a simulation performed with the advanced calculation model.

### 3.3 The MACS+ software

This software is directly based on the simple method developed by Bailey and Moore. It has the additional feature that it calculates the temperatures that are needed to apply the simple method: on

---

<sup>10</sup> Even if the method has been calibrated.

<sup>11</sup> Even if advanced model is used to determine the temperatures.

<sup>12</sup> The Authors used the software VULCAN

the upper side of the slab, on the lower side of the slab, at the level of the reinforcement and in the unprotected steel beams.

This software is easy to install and easy to use. It is robust and, as far as we could verify, it is based on a correct implementation of the Bailey-Moore method in which some considerations from the Eurocodes, such as material laws or partial safety factors, have been implemented.

Compared to a manual application of the method which bears important risks of human errors (because some of the equations are long and quite complicated), this software is certainly a significant improvement and can make it a tool of choice for applying the simple Bailey-Moore method.

We found that the user can make an error in the introduction of the data that is not prevented in the software. This error is linked to the choice of decimal separator and may lead to a wrong loading being considered in the calculation. Based on our finding that we communicated to the authors, this problem has been fixed in the latest version 3.0.2 of the software. It is nevertheless still possible to download the previous uncorrected 3.0.1 version.

In short, if the simple Bailey-Moore method has to be applied, this software is certainly a good tool. It is remarkable to note that, in the “Help –About” menu of the software, MACS+ is described as a “*pre design software*”. This is in fact exactly our conclusion mentioned in the last sentence of Section 3.2.

### 3.4 Numerical modelling

Numerical modelling is based on acknowledged principles of structural mechanics and should therefore provide a “correct” solution of the problem for each design. Our simulations and some comparisons with simulations performed with other software have yet shown that it could be wise to give some recommendations about good practice of numerical modelling of slab panels in tensile membrane action. The response may indeed be particularly sensitive to the amount of tensile strength of concrete, to the constitutive model of concrete in tension and to the constitutive model of steel in the reinforcing bars, with the ductility being of primary importance for both constitutive models. Designers who have but their experience on models made for other more traditional types of structures may not be aware of the overwhelming influence of these parameters in tensile membrane action because the influence is not so pronounced in traditional structures.

We also found that the simple equation D.15 of EN 1994-1-4 should not be applied in tensile membrane action if the ribs of the slabs are modelled by an equivalent layer of concrete. This is because this equation has been tuned to give a good estimation of the temperature on the unexposed side of the slab (in order to judge about the insulating criteria *l*) whereas the temperature at the level of the steel mesh is more relevant in tensile membrane action. In our example, the thickness of the equivalent layer was lower than that given by equation D.15.

## 4 Bibliography

Bailey C G & Moore D B (2000), *The structural behaviour of steel frames with composite floorslabs subject to fire: Part 1: Theory*, The structural engineer, Vol 78, N°11, 19-27

Bailey C G & Moore D B (2000), *The structural behaviour of steel frames with composite floorslabs subject to fire: Part 2: Design*, The structural engineer, Vol 78, N°11, 28-33

Bailey C G, White D S & Moore D B (2000), *The tensile membrane action of unrestrained composite slabs simulated under fire conditions*, Engineering Structures, 22, 1583-1595

Bailey C G (2001a), *Membrane action of unrestrained lightly reinforced concrete slabs at large displacements*, Engineering Structures, 470-483

Bailey C G (2001b), *Steel structures supporting composite floor slabs: design for fire*, BRE, Digest 462

Bailey C G (2003), *Efficient arrangement of reinforcement for membrane behaviour of composite floor slabs in fire conditions*, J. of Constructional steel research, 59, 931-949

Bailey C G (2004), *Membrane action of slab/beam composite floor systems in fire*, Engineering Structure, 26, 1691-1703

Bailey C G & Toh W S (2007), *Behaviour of concrete floor slabs at ambient and elevated temperatures*, Fire Safety Journal, 42, 425-436

Bailey C G & Toh W S (2007), *Small-scale concrete slab tests at ambient and elevated temperatures*, Engineering Structures, 29, 2775-2791

Burgess I & Huang S S (2015), *Tensile Membrane Action and the Performance of Composite Slabs in Fire*, submitted for publication

Foster S G, Bailey C G, Burgess I W & Plank R J (2004), *Experimental behaviour of concrete floor slabs at large displacements*, Engineering Structures, 26, 1231-1247.

Gernay, T., Millard, A. and Franssen, J.M. (2013), "A multiaxial constitutive model for concrete in the fire situation: Theoretical formulation", International Journal of Solids and Structures, 50(22-23), pp. 3659-3673

Giroldo F & Bailey C G (2008), *Experimental bond behaviour of welded mesh reinforcement at elevated temperatures*, Magazine of Concrete Research, 60, 23-31

Hayes B, Ph. D. thesis

Here are the roots of the B-M method, as far as room temperature behavior is concerned. In fact, Hayes proposes two set equations: one when no tension crack is apparent along the yield lines on the top surface of the slab and one when tension cracks are penetrating the top surface. The B-M method is based on the first set of equations.

Note: one typing error in Eq. (2.68):  $4n^2a^2$  should be  $4na^2$

Hayes B (1968), *Allowing for membrane action in the plastic analysis of rectangular reinforced concrete slabs*, Magazine of concrete research, Vol. 20, N° 65, 205-212

Huang Z, Burgess I, Plank R & Bailey C (2004), *Comparison of BRE simple design method for composite floor slabs in fire with non-linear FE modelling*, Fire and Materials, 28, 127-138

Kemp K O (1967), Yield of a square reinforced concrete slab on simple supports, allowing for membrane forces, *The structural engineer*, N°7, Vol 45, 235-240

Sawczuk A & Winnicki L (1965), *Plastic behavior of simply supported reinforced concrete plates at moderately large deflections*, *Int. J. Solid Structures*, Vol. 1, 97-111

Vassart O & Zhao B (2013), *Membrane action of composite structures in case of fire*, *ECCS TC3 Fire Safety*, PP 235.

## 5 Annex: problems in the Bailey Moore simple calculation method

This method is not fool proof with regards to first principles of structural mechanics.

- 1) It is based on some kinematic considerations and, on the same time, on static equilibrium equations. Normally, ultimate load bearing capacity calculated according to the theory of plasticity is based purely on kinematic considerations or on static equilibrium equations. It is thus possible, when one of these approaches is being used, to know whether the results obtained are bigger or lower than the “true” load bearing capacity. This is not the case with the present approach.

It has to be mentioned that, in a case when the result of the simple method matches relatively well the result of the numerical simulation, the displacement that is evaluated in the simple method and that is a key component of the method was significantly smaller than the one calculated by the advanced method, see Figure 31. This tends to confirm that some approximations in the kinematic part of the method (for evaluating the displacement) are compensated other approximations in the static part of the method (in the equilibrium equations).

- 2) The deformation modes which are being considered are not cinematically admissible. The slab panel is assumed to deform according to rigid plates turning around linear yield lines<sup>13</sup> whereas the amplitude of the deformation is assumed to be formed of the addition of a circular line (thermal deformation) and a parabolic curve (effect of the stress related strain). Furthermore, the deflection caused by thermal gradients is assumed to be half the value of the thermal deformation that would occur in a uniaxial situation in the direction of the shortest span; this ratio of  $\frac{1}{2}$  is constant, irrespective of the aspect ratio of the slab panel, which is not correct.
- 3) The stress distribution is not statically admissible.
  - a. The stress distribution in the composite slab is evaluated as if there is no steel beam in the slab panel.

---

<sup>13</sup> Which is contradicted by experimental tests as well as by numerical modelling

- b. The contribution of the unprotected steel beams is evaluated independently, assuming that they are subjected to bending moment, without any consideration for the tensile membrane action in the slab panel.
  - c. As a result of points a. and b., in the center of the slab, concrete is simultaneously in tension under tensile membrane action and in compression in the composite action of unprotected steel-concrete beams.
  - d. The composite action in the perimeter beams and the stresses that it induces in the concrete slab are not considered in the equilibrium equations of the method but the full resistance to compression is considered when considering possible failure by compression in the concrete.
- 4) The load bearing capacity of the slab panel as a single structure cannot be evaluated directly. The load bearing capacity of the triangular part is evaluated first and the load bearing capacity of the quadrilateral part is evaluated independently. Both values generally are different. If the different part would carry the loads in series, the load bearing capacity of the system would be the lowest one of those calculated. But this is not the case here; all the different parts fail simultaneously when the whole slab panel fails. The simple method reconciles the difference in load bearing capacity of the different parts by an interpolation function without providing any justification.
- 5) Several hypotheses are embedded in the method, without any justification.
- a. The membrane force is equal in all yield lines at the point where they meet.
  - b. The compressive stress block depth is equal to 0,45 when failure by compression can occur.